

Chapter VII  
JUNCTIONS

## CHAPTER - VII

## JUNCTIONS

## INTRODUCTION :

The photovoltaic cell is one of the most important optoelectronic devices. Optoelectronic devices include those which convert optical signals into electrical ones or vice versa and those which detect optical signals through electronic processes. Electroluminescent <sup>de-vice,</sup> and photodetectors are also optoelectronic devices.

In an electroluminescent device, when a current or voltage is applied, it emits incoherent spontaneous emission with a wide spectral line-width ( $\sim 100 \text{ \AA}$ ). Among photodetectors there are (1) photoconductors which are used for infrared detection (2) Depletion-layer photodiodes used for high speed coherent and incoherent detection (3) Avalanche photodiodes which are promising solid-state detectors because of their internal current gain.

A photovoltaic cell converts light energy into electrical energy. When the absorption of radiation by a material causes the appearance of a potential difference between two portions of the material, the effect is known as photovoltaic effect. Phenomenologically one might consider the

photovoltaic effect to be the inverse process to electroluminescence. Photovoltaic conversion of photon energy appears to be one of the most promising ways of meeting the increasing energy demands of the future, (by way of using solar radiation as the incident energy source) in a time when conventional sources of energy are being depleted.

Thin film photovoltaic cells have been an intensive research area since most of the high energy solar flux is absorbed near the surface (of the order of two-three times the optical absorption length). In the case of thick crystals, the presence of deep lying junctions results in loss of generated carriers because of their recombination before reaching the junction. Hence shallow junctions are used to overcome this drawback. If small thickness is used, the surface recombination velocity will also need to be reduced, so as to allow the carriers to diffuse to the junction.

The other important advantages of thin film photovoltaic cells are :

1. Thin films can be deposited over a very large area.
2. The band gaps can be tailored.
3. Material requirement is very low due to the higher absorption coefficients compared to those of single crystals.
4. Deposition process is inexpensive and material cost is

also less as the material requirement is very less.

Basically photovoltaic conversion occurs through three separate processes.

1. Absorption of light to create electron-hole pairs in the appropriate semiconductor.
2. Collection and separation of these carriers by an electric field.
3. Distribution to an external load.

Most of the absorption and carrier generation occurs for photons of energy greater than the band gap of the material. Obviously for greater carrier generation and consequently higher photocurrent, the band gap energy should be small.

A photovoltaic cell consists of a potential energy barrier within a semiconducting material capable of separating the electrons and holes generated by the absorption of light within the semiconductors. Potential barriers may be caused due to :

- (a) difference in the conductivity type of the two materials used, e.g. a p-n junction.
- (b) the contact between a metal and semiconductor.
- (c) difference between the surface conductivity and volume conductivity of the material.
- (d) a junction between two semiconductors with an unequal band gap.

At least five different types of junctions can be enumerated, with a variety of combinations.

1. A material surface, representing a junction between a material and vacuum or a gaseous environment.
2. Junctions between two different metals with different work functions.
3. Schottky barriers (metal-semiconductor) : Junction between a metal and semiconductor.
4. Homojunction : Junction between two portions of the same material with different electrical properties ; most commonly, one being p-type and the other being n-type to form a p-n junction.
5. Heterojunction : junction between two different materials with different electrical properties.

A heterojunction is similar to a homojunction but the window is a layer of a larger band gap semiconductor to reduce surface recombination loss. In a heterojunction, two configurations are possible ; light incident through an electrode grid on the larger band gap material (called the backwall configuration) and through a grid on a thin layer of the small band gap material (called the front wall configuration)<sup>(1 - 4)</sup>.

**GENERAL DISCUSSION : SECTION - I****Heterojunctions :**

A junction formed between two semiconductors having different energy band gaps is termed as a heterojunction. If the conductivity type is the same in the two semiconductors the heterojunction is called an isotype heterojunction. An anisotype heterojunction is one in which the conductivity type is different in the two semiconductors<sup>(4)</sup>. Energy band scheme for description of photovoltaic effect is shown in Figure - 1. Under illumination a motion of electron minority carriers in the p-type portion of the barrier and a motion of hole minority carriers in the n-type portion across the barrier together constitute a current flow in the reverse direction of the barrier. If the junction is short circuited, the sum of these two currents is the observed short circuit current  $I_{sc}$ . If the junction is open circuited, a voltage is built up across the junction just sufficient to counter balance the current flow  $I_{sc}$ . The maximum value this  $V_{oc}$  can obtain is  $V_{max}$ , the difference between the location of Fermi levels in the two portions of the material before contact. This difference itself approaches an upper limit-the band gap of the material<sup>(5)</sup>.

Some of the requirements for forming a good quality photovoltaic heterojunction are

1. Band gap of small band-gap material : Band gap near 1.4 eV to maximize absorption of solar radiation (for solar

energy conversion) while minimizing diode current that limits  $V_{OC}$ . Direct optical absorption so that carriers are generated close to the junction. Long minority carrier diffusion length.

2. Band gap of larger band gap material : As large as possible while maintaining low series resistance.
3. Conductivity type : Small band gap material should usually be p-type because of longer electron diffusion lengths.
4. Electron affinities : Materials should be chosen such that no potential spike occurs at the junction for the photoexcited minority carriers.
5. Diffusion voltage : As large as possible, since the maximum  $V_{OC}$  is proportional to the diffusion voltage.
6. Lattice mismatch : As little mismatch in lattice constants of the two materials as possible.
7. Deposition methods : Suitable deposition methods for thin film formation and control should be available.
8. Electrical contacts : It should be possible to form low resistance electrical contacts to both n- and p-type materials.

There has been an interesting report on  $\text{SnSe-SnSe}_2$  eutectic crystals by W.Albers<sup>(6)</sup>. He has found the alloy to have a lamellar structure in the form of alternate SnSe and

SnSe<sub>2</sub> lamellae of p and n type, respectively. Thus the eutectic crystals have a high junction density, about  $10^3 - 10^4 \text{ cm}^{-1}$ , with a good structural matching across the junctions. These facts indicate the SnSe-SnSe<sub>2</sub> heterojunctions interesting enough for photovoltaic studies. The optical absorption coefficients of SnSe and SnSe<sub>2</sub> have also been reported to be high, namely, about  $10^4 \text{ cm}^{-1}$ . The author in his studies on thin films of these compounds has also observed the same order of the absorption coefficients. The electrical conductivity values of SnSe, SnSe<sub>2</sub> and SnSe-SnSe<sub>2</sub> eutectic crystals are of the order of  $5 \text{ (ohm-cm)}^{-1}$ ,  $2.5 \text{ (ohm-cm)}^{-1}$  and  $0.11 \text{ (ohm-cm)}^{-1}$ , respectively, as found by the author. SnSe has a p-type conductivity and SnSe<sub>2</sub>, n-type conductivity. The band gaps of SnSe and SnSe<sub>2</sub> films are about 0.94 eV and 1.36 eV. The mobility and carrier concentrations of SnSe solid state reacted films were found to be  $115 \text{ cm}^2/\text{Vs}$  and  $2 \times 10^{16} \text{ cm}^{-3}$ , respectively and for SnSe films directly evaporated from the compound, these were found to be about  $60 \text{ cm}^2/\text{Vs}$  and  $4 \times 10^{16} \text{ cm}^{-3}$ , respectively.

Bhatt et al<sup>(7)</sup> have studied the characteristics of SnSe/SnSe<sub>2</sub> heterojunctions. The electrical conductivities of SnSe and SnSe<sub>2</sub> thin films have been reported to be  $15 \text{ (ohm-cm)}^{-1}$  and  $2.05 \text{ (ohm-cm)}^{-1}$ , respectively. The band gap of SnSe was found to be about 0.95 eV and that of SnSe<sub>2</sub>, 1.1 eV. Both the materials have an absorption coefficient more than  $10^4 \text{ cm}^{-1}$ . The carrier mobilities of SnSe and SnSe<sub>2</sub> are  $154$  and  $27 \text{ cm}^2/\text{Vs}$ .

respectively. The  $V_{oc}$  of SnSe/SnSe<sub>2</sub> has been reported to be about 400 mV at 100 mW/cm<sup>2</sup> and  $I_{sc}$ , quite small, about 10<sup>-7</sup> A. Except this, the author has not come across any report related to such studies. This chapter reports on the fabrication and characterization of the heterojunctions : SnSe/SnSe<sub>2</sub>, p-Si/SnSe<sub>2</sub>, n-Si/SnSe and also of metal-semiconductors.

### Experimental Results :

SnSe solid state reacted films were deposited on aluminium coated glass substrates (aluminium as an ohmic electrode) and over them, SnSe<sub>2</sub> films were deposited. Finger shaped aluminium electrodes were evaporated over the SnSe<sub>2</sub> layers using suitable masks. The configuration of SnSe/SnSe<sub>2</sub> is shown in Figure - 2. Similarly, p-Si/SnSe<sub>2</sub> and n-Si/SnSe were also prepared and their characteristics were studied. The measurements were made in dark as well as under illumination with a 100 Watt lamp.

#### 3.1 Current-Voltage Characteristics :

Upon applying a voltage in dark across the sandwich structure of the cell, the resultant currents observed were low and stable with time. However, with increase in the voltage the current also increased with a tendency to vary with time which may be due to development of space charge. Figure - 3,4,5 show typical dark current voltage characteristic curves for SnSe/SnSe<sub>2</sub>, p-Si/SnSe<sub>2</sub>, n-Si/SnSe samples, respectively. Both

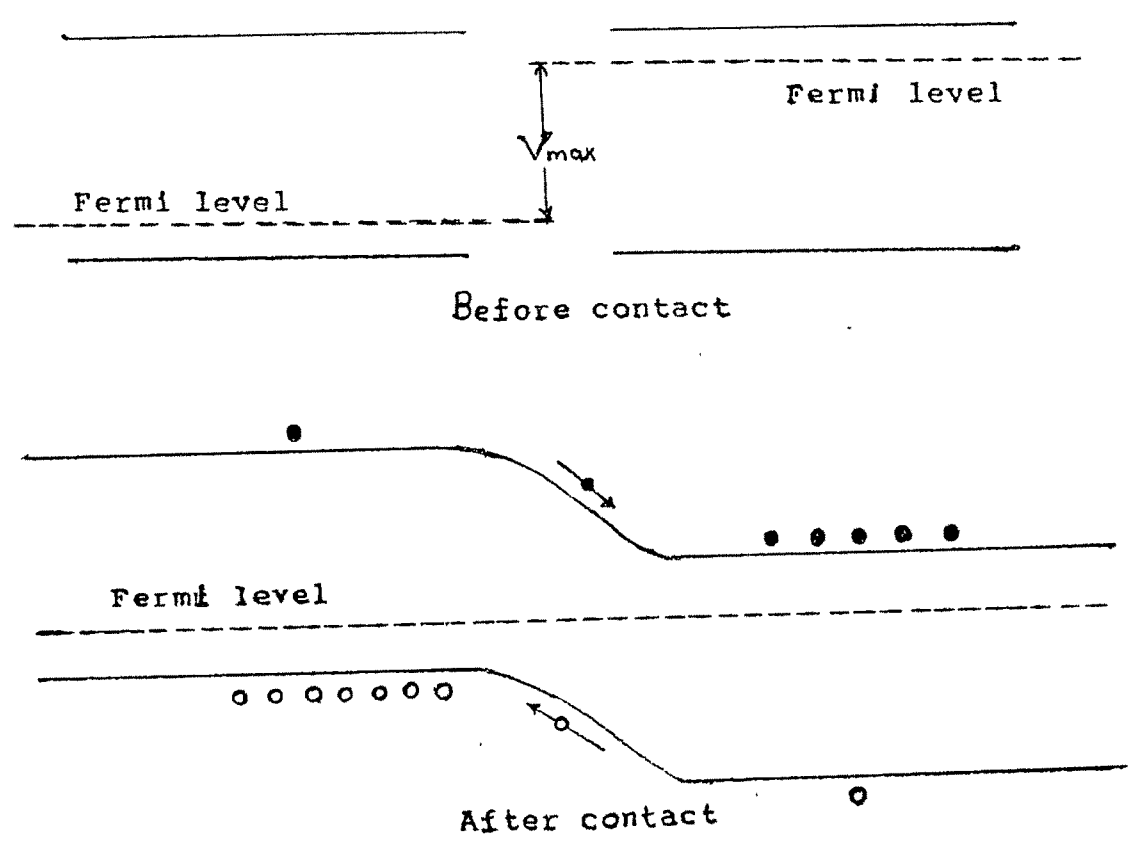


Figure - 1 : Energy-band diagram for description of Photovoltaic effect.

- |                   |                     |
|-------------------|---------------------|
| 1 Glass substrate | 4 SnSe <sub>2</sub> |
| 2 Al electrode    | 5 Al electrode      |
| 3 SnSe            |                     |

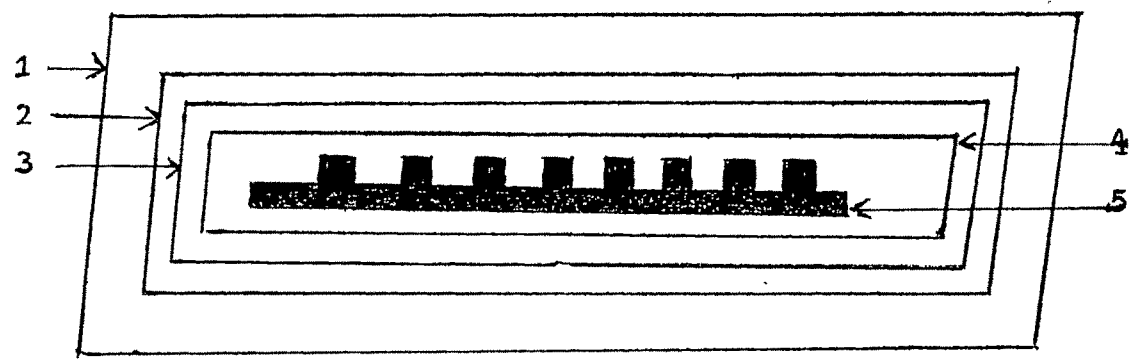


Figure - 2 : Configuration of SnSe/SnSe<sub>2</sub> heterojunction.

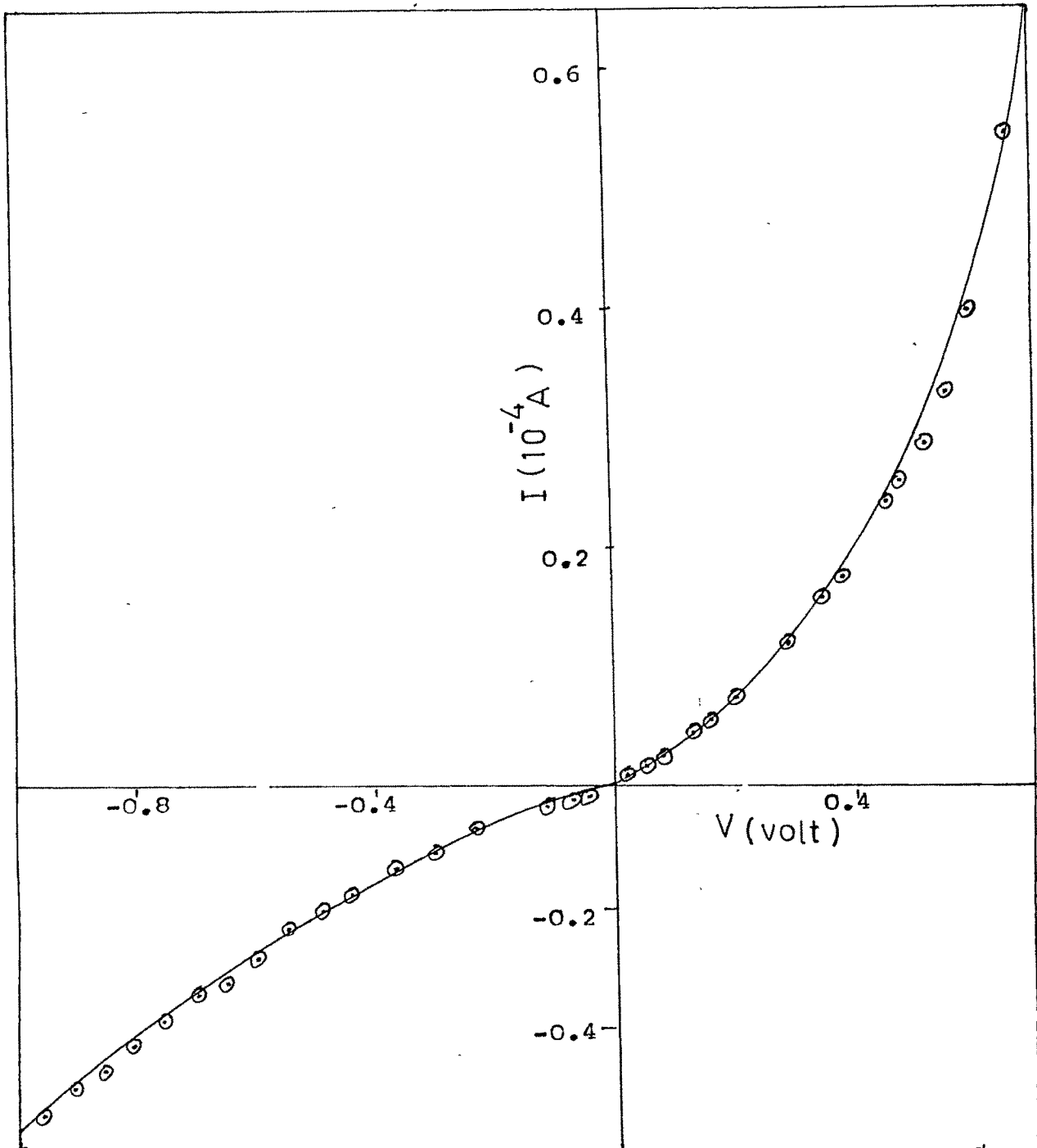


Figure - 3 : I - V Characteristics ; SnSe/SnSe<sub>2</sub> junction.

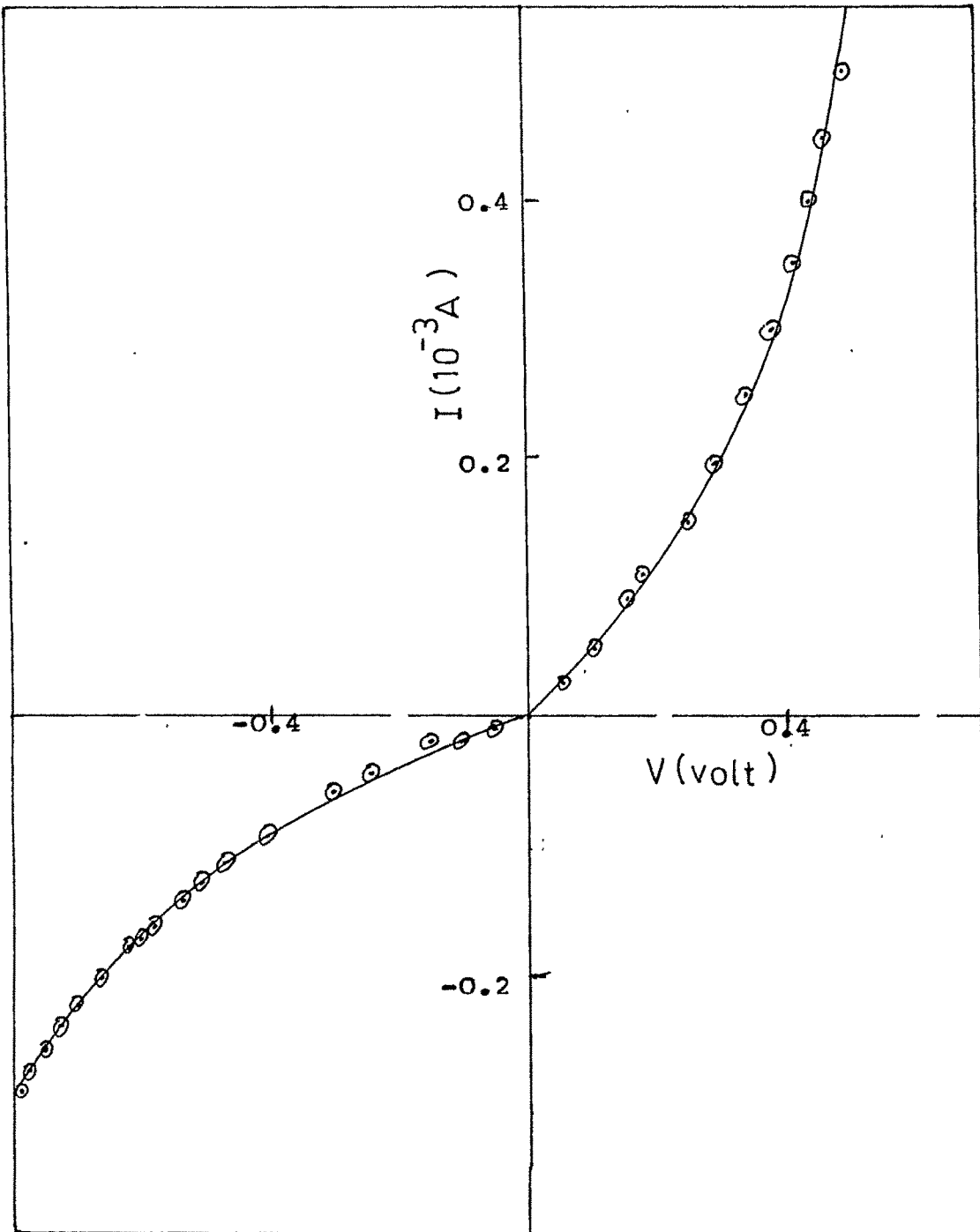


Figure - 4 : I - V characteristics ; p-Si/SnSe<sub>2</sub> junctions.

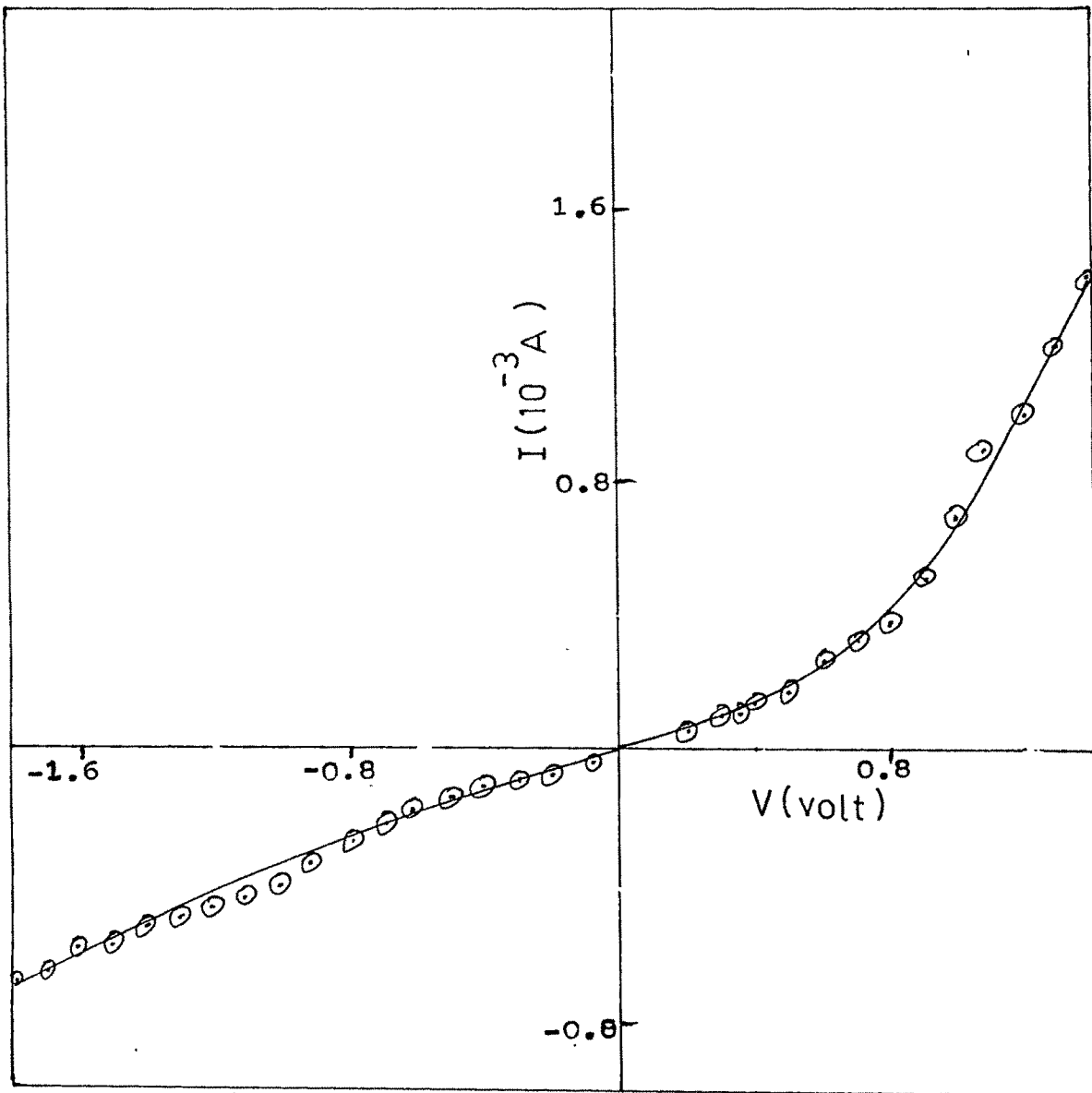


Figure - 5 : I - V Characteristics ; n-Si/SnSe junctions.

the forward and reverse bias characteristics are shown in the figures. For the same applied voltage, the current in the forward bias is more than in the reverse bias. In the reverse bias it is observed that the current did not saturate and it is found to increase with applied voltage. In the low voltage region, the observed curve can be fitted to an expression of the form.

$$I = I_0 \exp \left( \frac{-qV}{nKT} \right) \quad \dots 1$$

where  $I$  is the measured current,  $I_0$  is the reverse saturated current,  $K$  is the Boltzmann constant,  $T$  is the absolute temperature and  $n$  is the ideality factor. The plot of  $\log I$  vs  $V$  is shown in Figure - 6. The linear nature of the plot is in agreement with the above relation. The slope of the straight line gives the ideality factor  $n$ .

Two of the most important parameters which play an important role in the device performance are the series resistance  $R_s$  and the shunt resistance  $R_{sh}$ . A convenient technique to determine  $R_s$  is to obtain it from the linear part of the  $I - V$  characteristics for forward bias. The inverse of the slope yields  $R_s$  and  $R_{sh}$  can be obtained as inverse of slope of  $I - V$  curve in the 3rd quadrant, i.e., reverse bias. The series resistance  $R_s$ , shunt resistance  $R_{sh}$  and the ideality factor  $n$

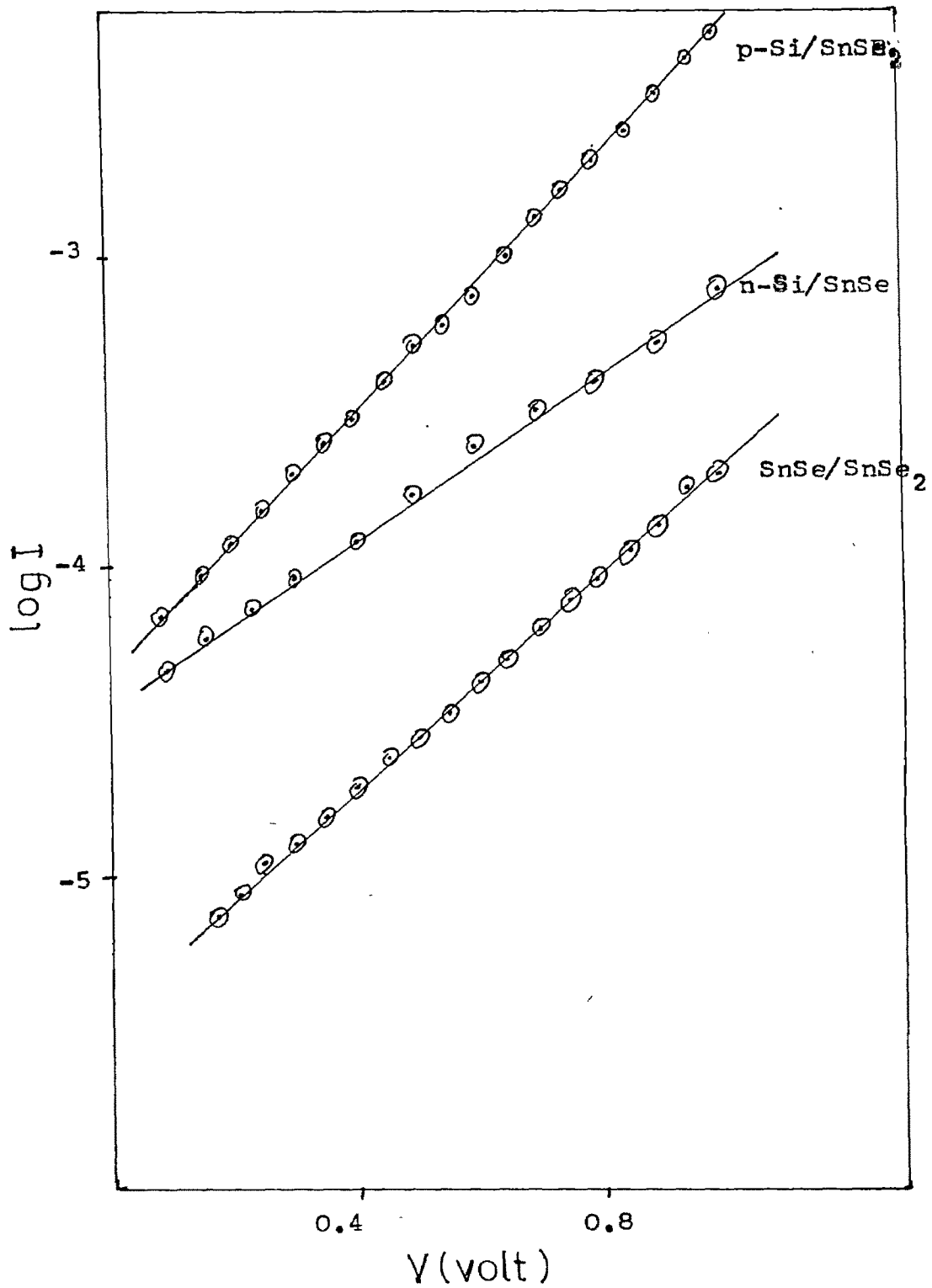


Figure - 6 : Plot of  $\log I$  vs  $V$  for Heterojunctions indicated.

obtained for SnSe/SnSe<sub>2</sub>, p-Si/SnSe<sub>2</sub> and n-Si/SnSe, are listed in Table - 1.

*not reported with or for 192*

Junction	R <sub>s</sub> (KΩ )	R <sub>sh</sub> (KΩ )	n
SnSe/SnSe <sub>2</sub>	5.0	10.0	5.2
p-Si/SnSe <sub>2</sub>	0.57	0.8	3.8
n-Si/SnSe	0.5	2.5	7.6

Similar results have been reported by Bhatt et al for the SnSe/SnSe<sub>2</sub> junction. Others too have reported such results, e.g. for CuInSe<sub>2</sub>/InTe<sup>(8)</sup> and Cu<sub>2</sub>S/CdS junctions<sup>(9)</sup>. Their ideality factors are less compared to the present case. The values of R<sub>s</sub> for SnSe/SnSe<sub>2</sub> and n-Si/SnSe in the present study are about 10<sup>3</sup> ohm which is lower than the values reported by Bhatt et al for the SnSe/SnSe<sub>2</sub> junction by an order of 100. This may be due to low resistivity of the SnSe films which are obtained by solid state reaction in the present work. On the other hand, R<sub>sh</sub> is of the order of Kilo ohms which is less than the values obtained by Bhatt et al. Particularly, it is less by an order of 100 compared to the values reported for SnSe/SnSe<sub>2</sub> by Bhatt et al, indicating high leakage rates dominating the junction.

In an ideal case,  $R_s \rightarrow 0$  and  $R_{sh} \rightarrow \infty$ , i.e. there is no resistance loss. The major contributions to the  $R_{sh}$  are by the film resistance of the semiconducting material making up the cell, the resistance of the metallic contact and interconnection and contact resistances between metallic contacts and semiconductors. The  $R_s$  decreases with high doping levels and deep junctions which are just the opposite of the necessary condition for high current collection efficiency. A large  $R_s$  may also be due to the grid shadowing area which may be a large fraction of the active area of the cell. It is also affected by the grain size. In the present case,  $R_s$  is high which may be basically due to large resistivity of the semiconducting films forming the junction. The increase in the resistance may also be due to large resistance of the front grid structure and the contact resistances. The resistance loss is distributed within the film.  $R_s$  depends on the dimensional geometries and the increase in  $R_s$  may also be due to the increase in the collection efficiency by shallow junction depth and also may be due to small band gap of the window material.

$R_{sh}$  is mostly caused by leakage across the junction around the edge of the cell. The shunting currents may also arise from other modes of transport such as surface conduction by recombination/generation or tunnelling at the periphery of the junction plane or tunnelling currents at three dimensional imperfections in the junction plane<sup>(4)</sup>.

According to Hovel<sup>(10)</sup>, a low value of  $R_{sh}$  is also responsible for higher values of  $n$ . According to him, values of  $n$  close to 1 are almost certainly due to dominance of injected current (due to the injection of minority carriers from top region into the base) and values close to 2 are most likely to be due to space charge region recombination of partly injected holes and electrons within the depletion region, or due to the recombination at the edge of the device within the space charge region. Both these mechanisms can exhibit  $n$  in the range of 1 to 2. The  $n$  values in the present case are high which may be indicative of the reduced density of recombination centres. Similar results have also been reported by Shockley et al<sup>(11)</sup> in the case of Si junction solar cell. A variety of physical processes can contribute to 'n' values different from unity. These include tunnelling through the barrier, intermediate layer with new dielectric and transport properties and recombination or trapping at states near the interface and within the semiconductor band gap. The chemical structure at the interface also influences the value of  $n$ .

#### Short Circuit Current :

The short circuit current  $I_{sc}$  is the current that flows through the junction under illumination at zero applied bias and in the ideal case (when  $R_s$  and  $R_{sh}$  resistance effects are not

present) is equal to the light generated current,  $I_L$ , and proportional to the incident number of photons, i.e., the illumination intensity. The plots of  $I_{sc}$  vs intensity is shown in Figure - 7 for SnSe/SnSe<sub>2</sub>, p-Si/SnSe<sub>2</sub> and n-Si/SnSe, respectively. It is observed that  $I_{sc}$  increases with the intensity in all the cases.  $I_{sc}$  reported by Bhatt et al for SnSe/SnSe<sub>2</sub> is  $6.4 \times 10^{-7}$  A. The  $I_{sc}$  found in the present case at the same illumination intensity for SnSe/SnSe<sub>2</sub>, p-Si/SnSe<sub>2</sub> and n-Si/SnSe are  $3 \times 10^{-7}$  A,  $6.62 \times 10^{-7}$  A and  $1 \times 10^{-7}$  A, respectively.

#### Open circuit voltage :

The open circuit voltage  $V_{oc}$ , defined at zero current through the junction is given by the equation (assuming only one current mechanism)

$$V_{oc} = 1/A \ln [(I_{sc}/I_s)+1] \quad \dots 3$$

where  $A = q/nkT$ , a constant,  $I_s$  = saturation current. It might be assumed from equation (3) that high values of  $n$  would be desirable in obtaining high  $V_{oc}$  but this is not actually the case, since high  $n$  is usually associated with high values of  $I_s$  whereas  $V_{oc}$  is always higher for low values of  $n$  (12).

The  $V_{oc}$  of the junction is directly related to the band gap of the semiconductors through the energy barrier height of

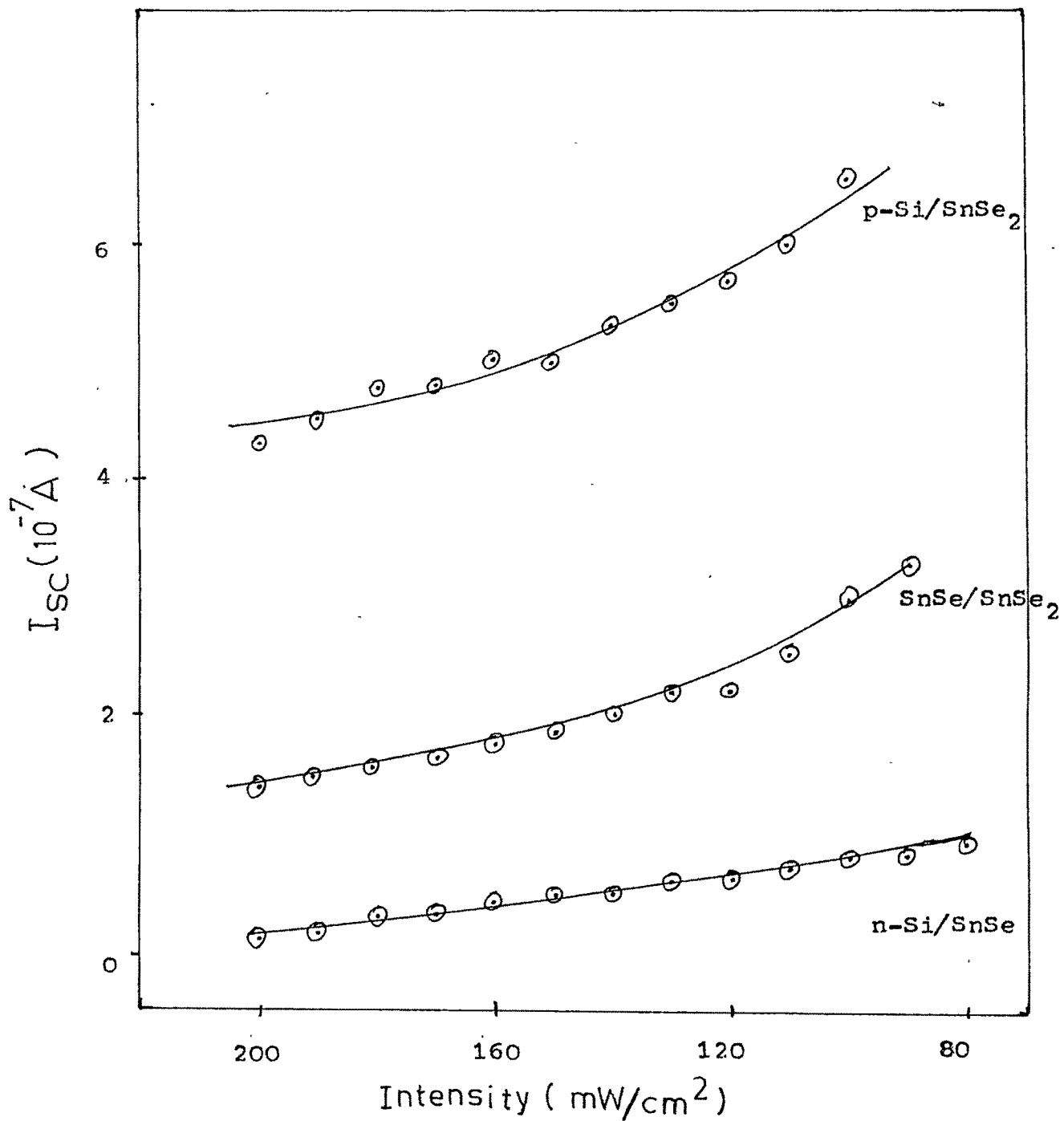


Figure - 7 : Plot of  $I_{sc}$  vs Intensity for heterojunctions indicated.

the junction. It is often written as a function of short circuit photocurrent,  $I_{sc}$ , the dark current,  $I_0$ , of the junction and ideality factor,  $n$  :

$$V_{oc} = nkT/q \ln [I_{sc}/I_0 + 1] \quad \dots 4$$

For a perfect junction,  $n$  is equal to 1 and  $V_{oc}$  attains its highest value ; while for large values of  $n$ ,  $I_0$  is large in such a way that  $V_{oc}$  is reduced. The dark current  $I_0$  is mainly determined by the band gap of the material and the temperature.  $I_0$  decreases and  $V_{oc}$  consequently increases with increasing band gap and decreasing temperature. The plot of  $V_{oc}$  vs intensity for SnSe/SnSe<sub>2</sub>, p-Si/SnSe<sub>2</sub>, n-Si/SnSe is shown in Figure - 8. The  $V_{oc}$  and  $I_{sc}$  depend on the illumination intensity, as observed above. The  $V_{oc}$  obtained at 100 mW/cm<sup>2</sup> for the above mentioned respective junctions are 100 mV, 189 mV and 3 mV. The values reported by Bhatt et al for the SnSe/SnSe<sub>2</sub> junction is 385 mV at the same intensity. Thus it seems, while the solid state reacted SnSe film has decreased the series resistance significantly, it has <sup>not</sup> helped to improve the  $V_{oc}$  and, on the contrary the  $V_{oc}$  has quite decreased. This agrees with the theoretical result that  $V_{oc}$  is unaffected simply by the change in  $R_s$ . Probably  $R_s$  can affect the  $I_{sc}$  only, that too, when it is quite large<sup>(4)</sup>.

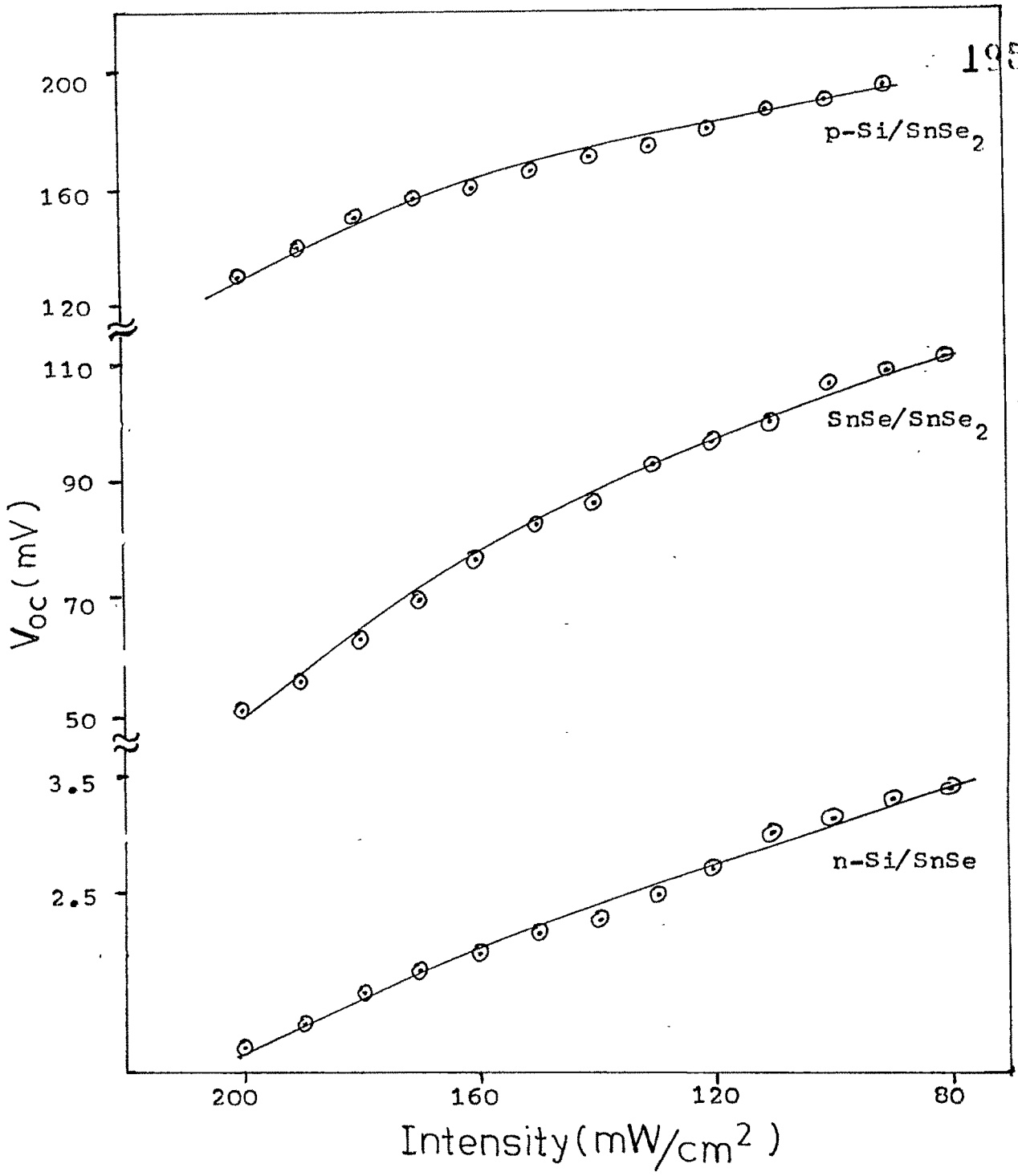


Figure - 8 : Plot of V<sub>oc</sub> vs Intensity for heterojunctions indicated.

**Power output :**

The power output from a photovoltaic cell is given by

$$P_m = I_m V_m \quad \dots 5$$

where  $V_m$  and  $I_m$  are the voltage and current, respectively, at maximum power.  $P_m$  can be calculated from the graph of  $I$  vs  $V$  under illumination.  $V_m$  and  $I_m$  can be determined by computing the product at various points along the curve and selecting the point where the product is maximum,  $P_m$ . The  $P_m$ , obtained from the  $I$ - $V$  curves (Figure - 9,10,11) are found to be  $1.27 \times 10^{-8}$ ,  $8.44 \times 10^{-8}$ ,  $1.24 \times 10^{-10}$  W for SnSe/SnSe<sub>2</sub>, p-Si/SnSe<sub>2</sub>, n-Si/SnSe, respectively.

**Fill factor :**

The fill factor,  $ff$ , which is defined as  $(V_m I_m)/(V_{oc} I_{sc})$  measures the squareness of the  $I$  -  $V$  curve. The two ratios  $V_m/V_{oc}$  and  $I_m/I_{sc}$  and the  $ff$  all improve with increasing values of  $V_{oc}$  and with decreasing values of  $n$  (diode ideality factor) and temperature. Higher band gap materials yield higher values of the ratios  $V_m/V_{oc}$  and  $I_m/I_{sc}$  and high fill factors because of their high  $V_{oc}$ . When  $R_s$  and  $R_{sh}$  effects cannot be neglected, the two ratios  $V_m/V_{oc}$  and  $I_m/I_{sc}$  and the  $ff$  are all reduced. For the three junctions studied, viz., SnSe/SnSe<sub>2</sub>, p-Si/SnSe<sub>2</sub>, n-Si/SnSe, the  $ff$ 's are found to be 0.424, 0.674 and 0.399, respectively. The  $ff$  reported by Bhatt et al for SnSe/SnSe<sub>2</sub> is 0.542. Thus it is seen that the p-Si/SnSe<sub>2</sub> junction again gives the maximum  $ff$  of the three junctions studied.

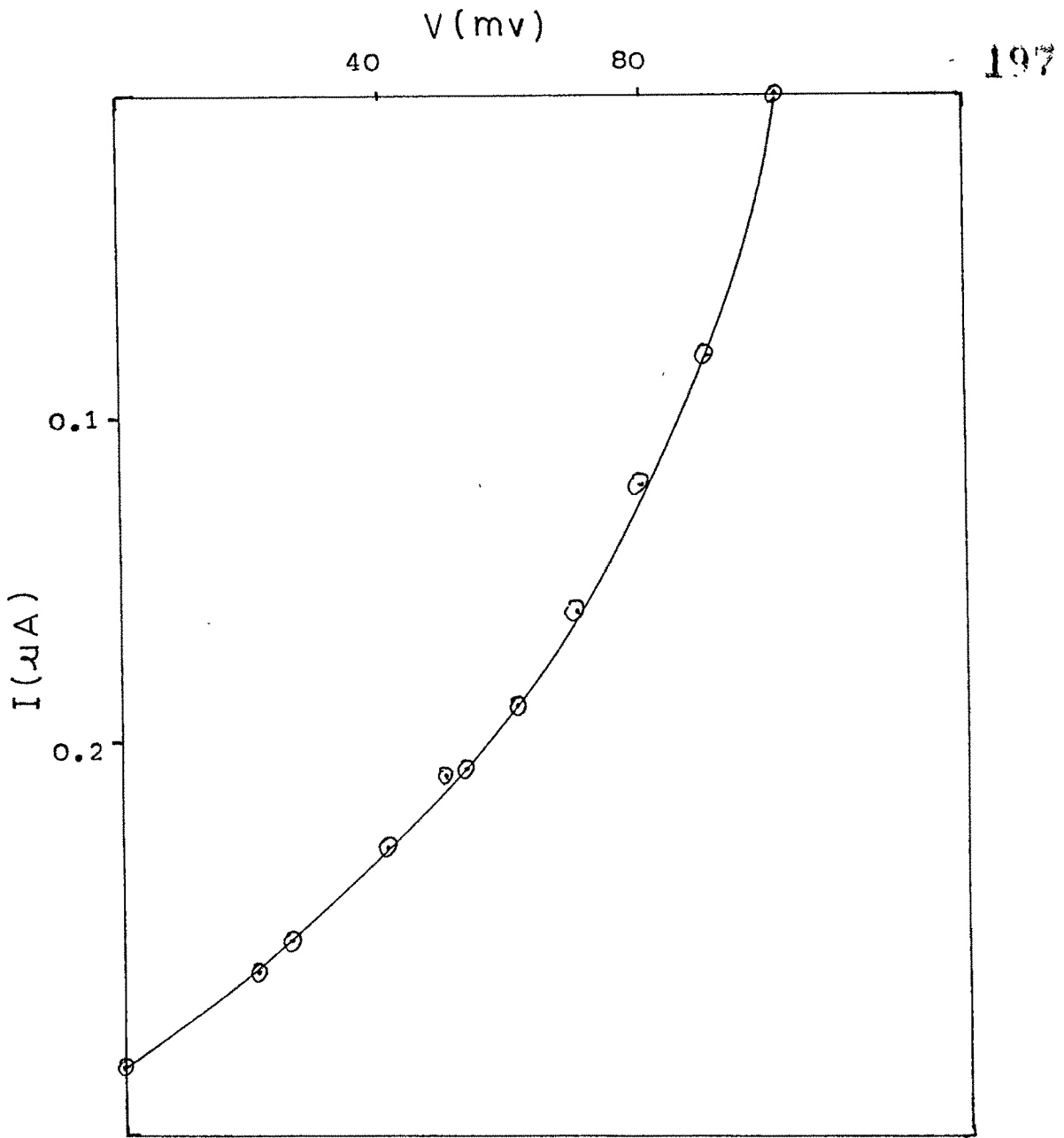


Figure - 9 : Voltage and current output from illuminated SnSe/SnSe<sub>2</sub> heterojunction. (Intensity  $\sim 100 \text{ mW/cm}^2$ )

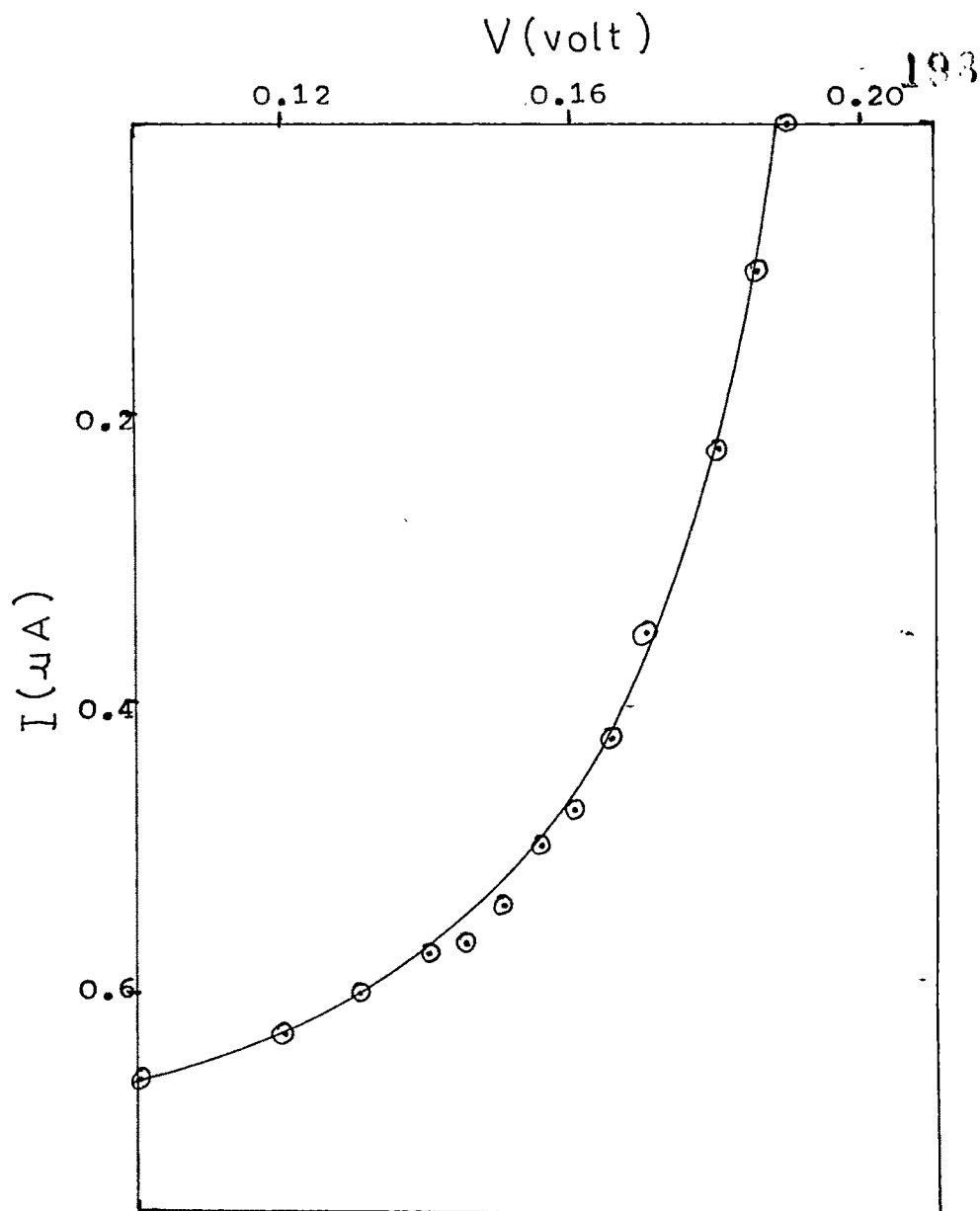


Figure - 10 : Voltage - current output from illuminated p-Si/SnSe<sub>2</sub> heterojunctions. (Intensity  $\sim 100\text{mW/cm}^2$ )

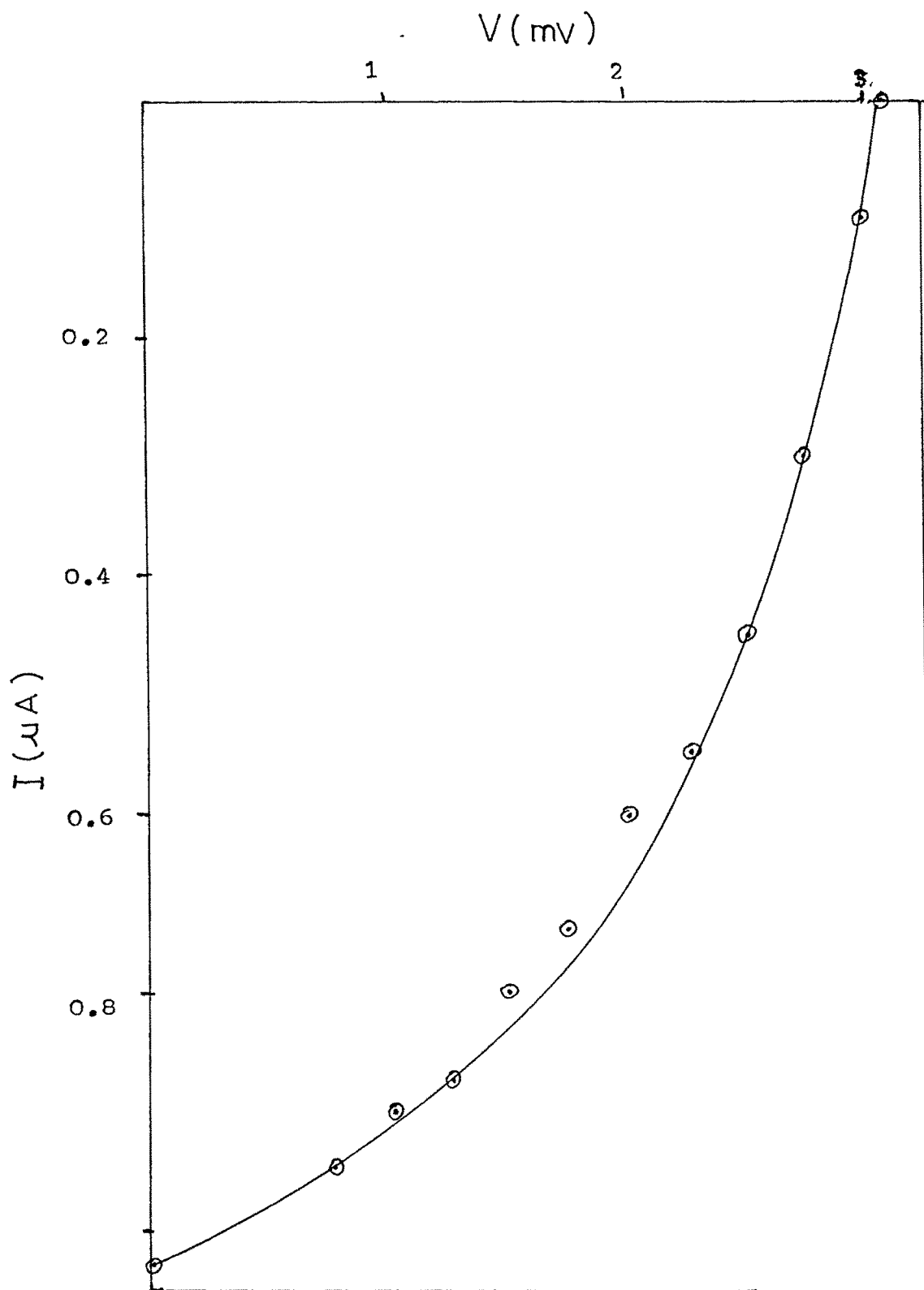


Figure - 11 : Voltage and current output from illuminated n-Si/SnSe heterojunction. (Intensity  $\sim 100 \text{ mW/cm}^2$ )

**Efficiency :**

The efficiency, of a photovoltaic cell in converting light into useful power is given by

$$\eta = \frac{V_m I_m}{P_{in}} \quad \dots 6$$

where  $P_{in}$  is the input power. The maximum output  $P_m$  is given by

$$P_m = V_m I_m = V_{oc} I_{sc} ff. \quad \dots 7$$

Therefore, the conversion efficiency of the cell is given as :

$$\eta = (V_{oc} \frac{I_{sc} ff}{P_{in}}) \times 100 \% \quad \dots 8$$

The efficiency is found to be  $1.54 \times 10^{-5}$ ,  $6.75 \times 10^{-5}$ ,  $9.9 \times 10^{-8}$  for SnSe/SnSe<sub>2</sub>, p-Si/SnSe<sub>2</sub>, n-Si/SnSe, respectively. The efficiency of a P - V cell depends critically on the imperfection concentration because of its effect on the minority carrier lifetime in the active layers. Not only is  $I_{sc}$  increased with increased life time but an increase in  $V_{oc}$  can be expected because of the decrease in  $I_o$ . Resistivity control is the second most important consideration. If the resistivity is decreased by heat treatment or by selecting proper thickness the efficiency can be increased. Low efficiency is partly caused by

the grain boundary effect and partly by poor quality of the semiconductor material grown on a foreign substrate. In the present case the efficiency is quite low the reasons for which may be (1) Thermal expansion coefficients of the two semiconductors may be very much different. (2) lattice mismatch (3) electron affinity mismatch, (4) high series resistance and, of course, quite a small band gap difference between the semiconductors used<sup>(13)</sup>.

#### C - V Characteristics:

The voltage dependence of junction capacitance is most commonly employed to study junction behaviour and to determine junction related parameters. Conventional C - V analysis essentially uses a measurement of the interfacial differential capacitance under reverse bias to obtain an estimate of the forward voltage which flattens the semiconductor bands. But it should be mentioned that C - V techniques do not measure the diffusion voltage directly but infers it from a measure of the reverse bias behaviour of the interface.

C - V measurement can be made point by point at different externally imposed bias values using capacitance bridge. It is known that for an abrupt p - n junction,

$$\frac{1}{C^2} = 2 \frac{[\epsilon_n N_n + \epsilon_p N_p] [V_d - V]}{q \epsilon_n N_n N_p \epsilon_p} \dots 9$$

where  $N$  is the impurity concentration,  $\epsilon$  is the dielectric constant,  $V_d$  is the diffusion potential difference (the built-in voltage) and  $V$  is the bias voltage. The subscripts  $p$  and  $n$  denote the values for  $p$  and  $n$  type semiconductors, respectively. From the above relation it is clear that the plot  $1/C^2$  vs  $V$  should be a straight line yielding the  $V_d$  as the intercept. Figures - 12,13,14 show the plots of  $C^{-2}$  vs bias voltage  $V$  for SnSe/SnSe<sub>2</sub>,  $p$ -Si/SnSe<sub>2</sub>,  $n$ -Si/SnSe heterojunctions, measured at room temperature and at 10 KHz frequency. The graphs show a good linearity. For higher reverse voltages, the slope of the line changes. It is likely that this change is due to electron quasi-Fermi level sweeping through deep donor traps below the conduction band edge<sup>(14)</sup>. The straight line nature of all the three plots, particularly at low moderate voltages, implies that the junction formed are of abrupt type. The diffusion voltages found for the three junctions, viz., SnSe/SnSe<sub>2</sub>,  $p$ -Si/SnSe<sub>2</sub> and  $n$ -Si/SnSe are 0.65 V, 0.75 V, and 0.6 V, respectively. In the case of SnSe/SnSe<sub>2</sub>, diffusion voltage is more than the value 0.4 V, reported by Bhatt et al.

## SECTION - II :

### METAL SEMICONDUCTOR JUNCTIONS :

In most of the applications in which electric fields are applied to semiconductors, some metallic contacts to the semiconductor must be made to act as electrodes. The electrical properties of such metal-semiconductor contacts have proved to

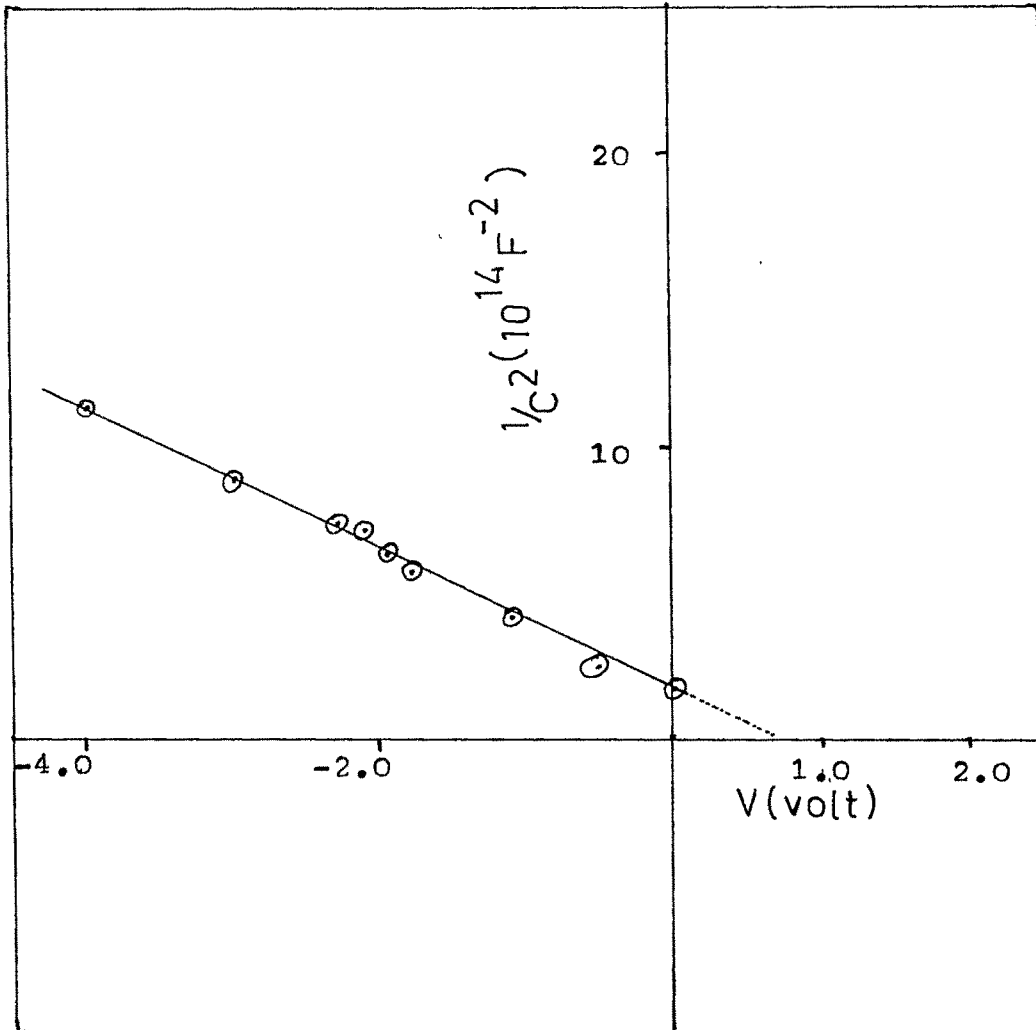


Figure - 12 : Plot of  $1/C^2$  vs  $V$  ; SnSe/SnSe<sub>2</sub> heterojunctions.

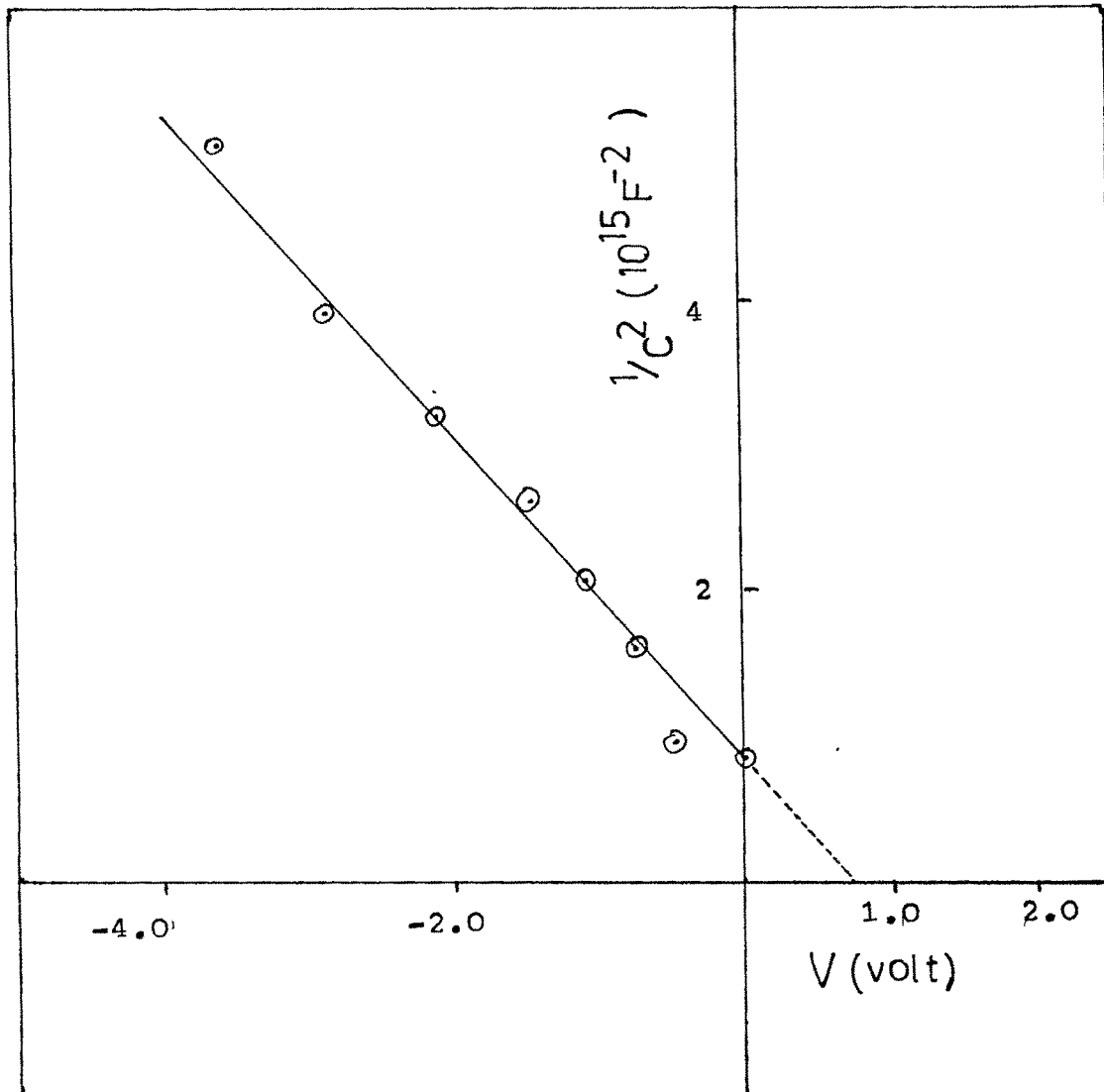


Figure - 13 : Plot of  $1/C^2$  vs  $V$  ; p-Si/SnSe<sub>2</sub> heterojunctions.

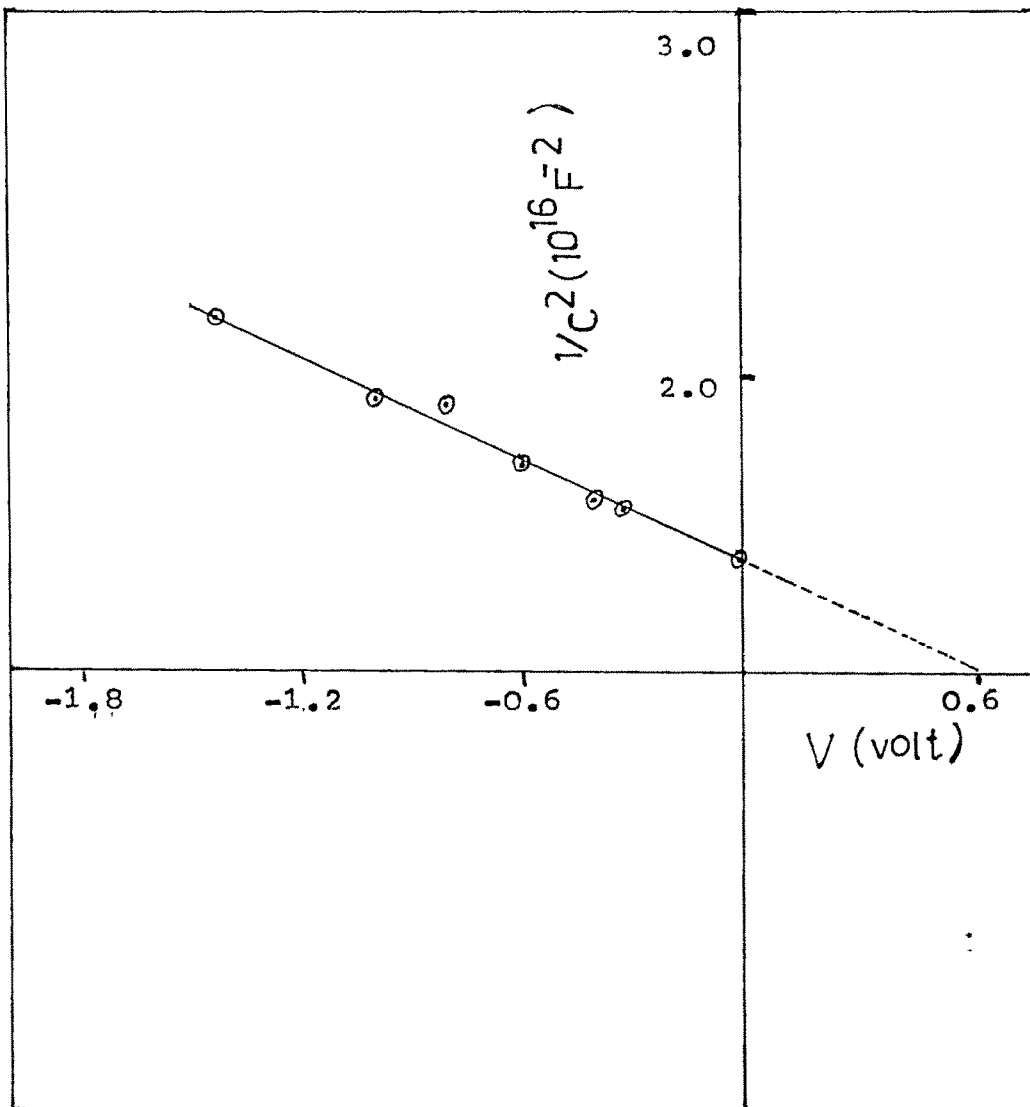


Figure - 14 : Plot of  $1/C^2$  vs  $V$  ; n-Si/SnSe heterojunctions.

have far more complex causes than was originally supposed. The simple model based on an ideal metal-semiconductor contact takes into account only the differences in the work functions of the metal and the semiconductor. Ideal metal-semiconductor contacts are ohmic when the charge induced in the semiconductor in aligning the Fermi level is provided by majority carriers. The band diagram is shown in Figure - 15.

The work function inequalities that determine junction behaviour, in the simple model, depend on the carrier type dominant in the semiconductor. If the semiconductor is n type,  $\phi_m > \phi_s$  gives a blocking contact and  $\phi_m < \phi_s$  gives an ohmic contact ; where  $\phi_m$  is the work function of the metal and  $\phi_s$  the work function of the semiconductor. On the other hand, if the semiconductor is p-type,  $\phi_m > \phi_s$  gives an ohmic contact and  $\phi_m < \phi_s$  gives a blocking contact. These criteria suffice apparently only to serve as guidelines to predict the nature of metal-semiconductor contacts.

Actually, however, chemical interactions on an atomic level between the specific metal and the specific semiconductor are often responsible to determine the overall contact properties at least as much as the differences in the work function.

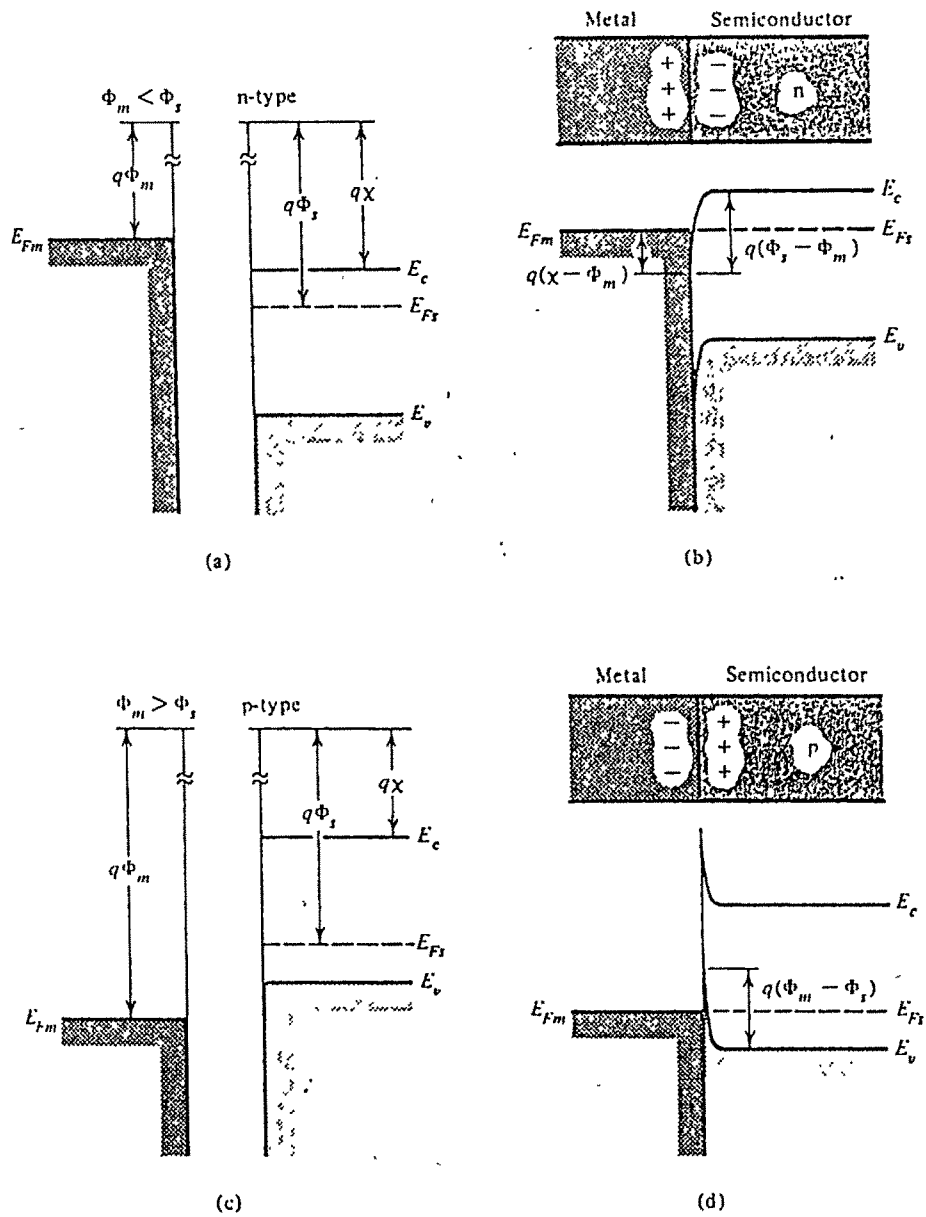


Figure -15 Ohmic metal-semiconductor contacts: (a)  $\Phi_m < \Phi_s$  for an n-type semiconductor, and (b) the equilibrium band diagram for the junction; (c)  $\Phi_m > \Phi_s$  for a p-type semiconductor, and (d) the junction at equilibrium.

In any case, there are two basic types of metal semiconductor contacts :

(1) Blocking or non-ohmic contacts which do not allow ready flow of electrons from the metal to the semiconductors, to balance space charge in the semiconductor.

(2) Ohmic contacts which allow such a ready flow of electrons. It is evident that in normal electrical measurements, where one desires an applied field to exist across the semiconductor and not across the metal-semiconductor junction, ohmic contacts are needed<sup>(1,15)</sup>.

For materials under present study, viz., SnSe and SnSe<sub>2</sub>, there are no reports found in literature on their metal semiconductor junctions. Hence their contacts with metals like Zn, Cd, Ni, and the metallic compound InBi were tested and the results obtained are discussed below.

#### **Experimental Results :**

The films, viz., those of SnSe and SnSe<sub>2</sub> were vacuum deposited on pre-evaporated Al films as ohmic electrodes. Over these films, small area circular deposits (about 5mm diameter) of the metals were prepared. The resulting structures were subjected to I-V and C-V characterizations.

### I-V Characteristics :

SnSe solid state reacted films and SnSe<sub>2</sub> films were deposited under different conditions (film thickness, substrate temperature). SnSe, (7 layer solid state reacted) films having thickness  $\sim 2100 \text{ \AA}$  were used since they were found to be of good crystallinity and high conductivity. Similarly, SnSe<sub>2</sub> films (thickness  $\sim 2000 \text{ \AA}$ ) deposited at substrate temperature of 200°C were used to form the junctions, since they were of good crystallinity and low resistivity (Chapter - 4).

The I - V characteristics of junctions of SnSe and of SnSe<sub>2</sub> with different metals were studied. Among these the structures Zn/SnSe, Zn/SnSe<sub>2</sub>, Ni/SnSe<sub>2</sub>, Cd/SnSe did not form the desired non-ohmic junctions as evidenced by the linear symmetric nature of the I-V plots. For example, a typical plot for Ni/SnSe<sub>2</sub> is shown in Figure - 16.

The structures In/SnSe, InBi/SnSe and Cd/SnSe<sub>2</sub> yielded non-ohmic I-V characteristics. Their respective I-V plots are shown in Figures - 17, 18 and 19. As can be seen, the forward and reverse bias curves are neither straight line nor symmetric. The  $R_s$  and  $R_{sh}$  values together with the values of the diode ideality factor of these junctions, obtained from these plots, are listed in Table - 2.

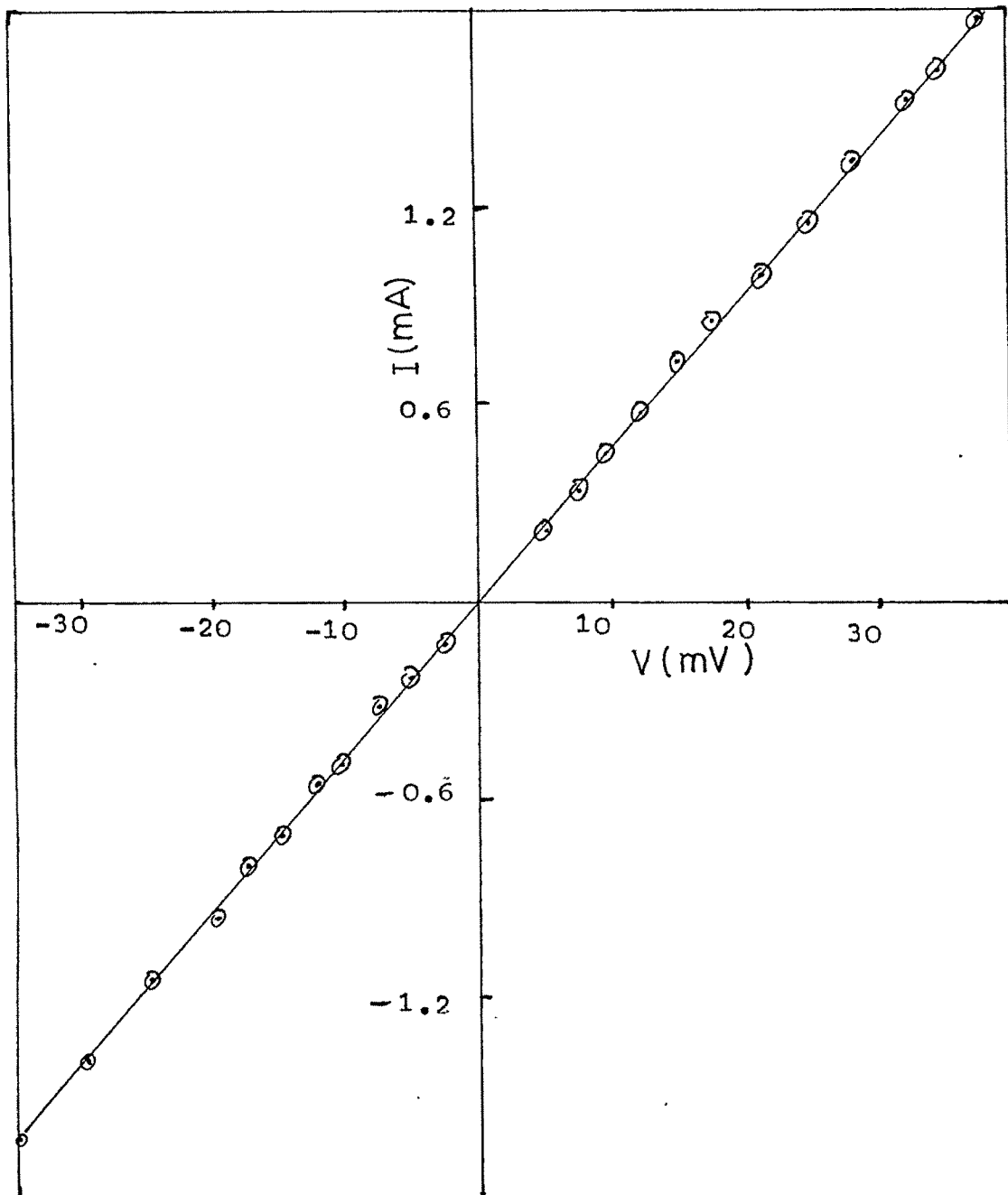


Figure - 16 : I - V characteristic of Ni/SnSe<sub>2</sub> junction.

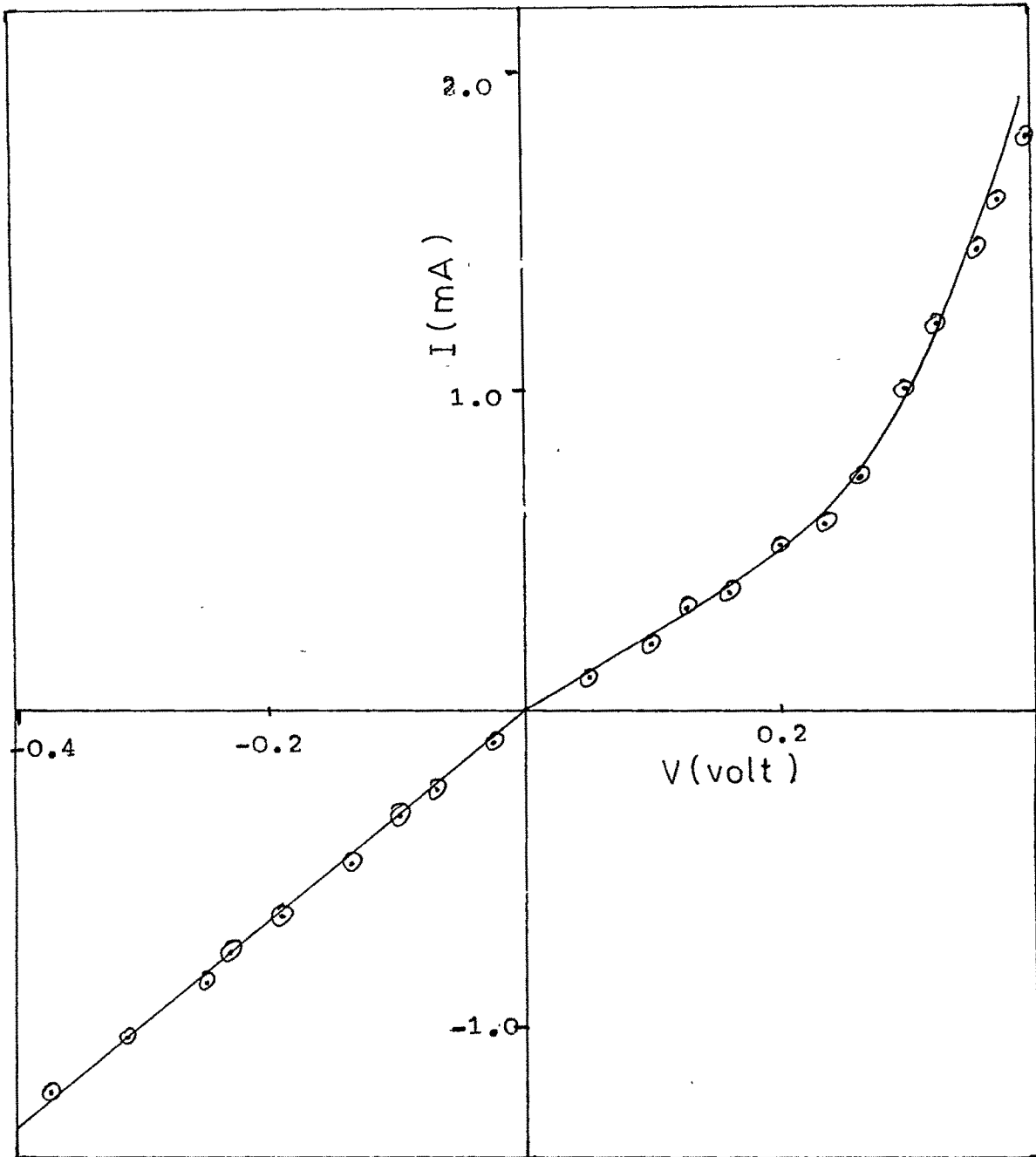


Figure - 17 : I - V characteristics of In/SnSe junction.

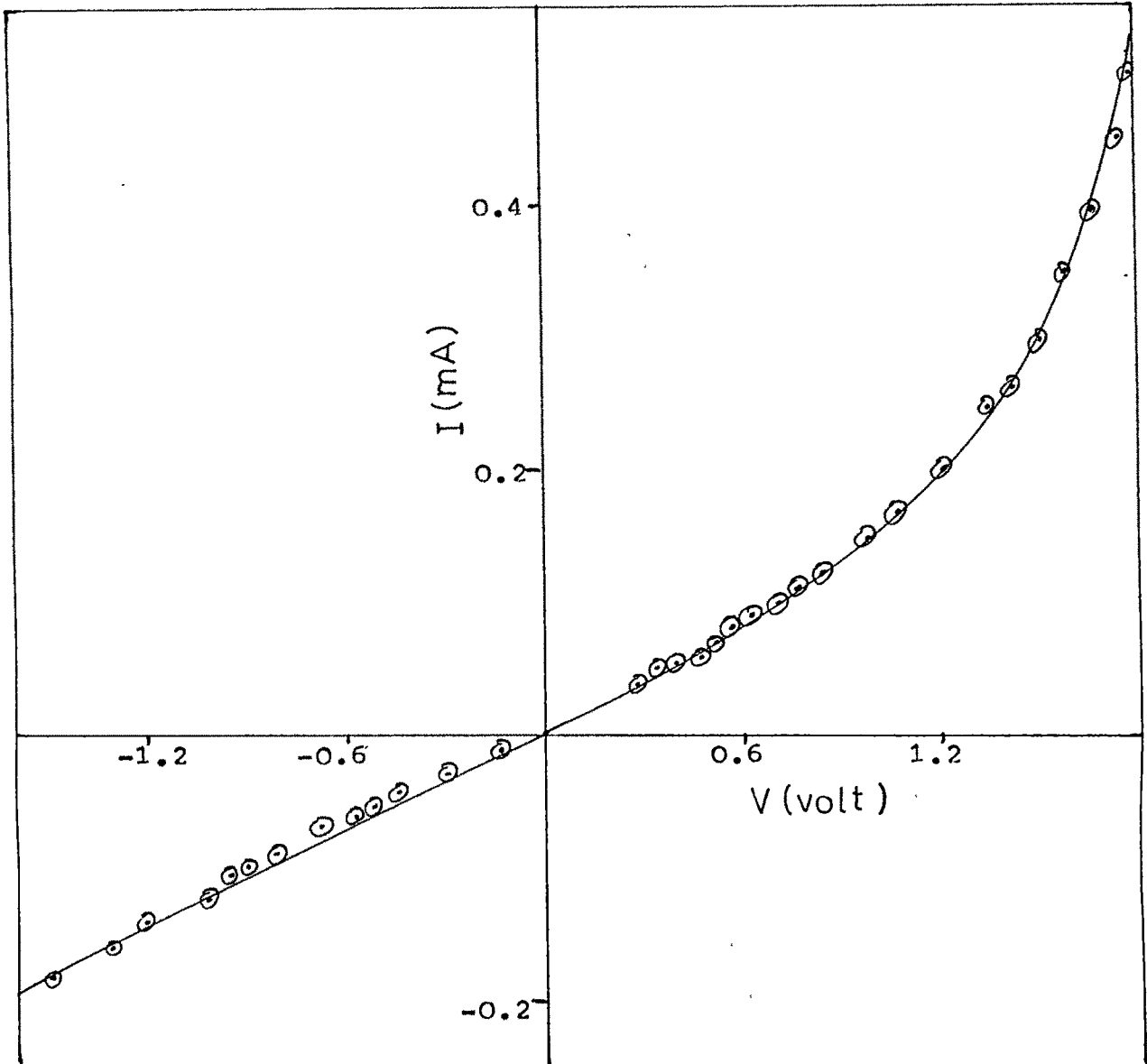


Figure - 18 : I - V characteristics of In-Bi/SnSe junctions.

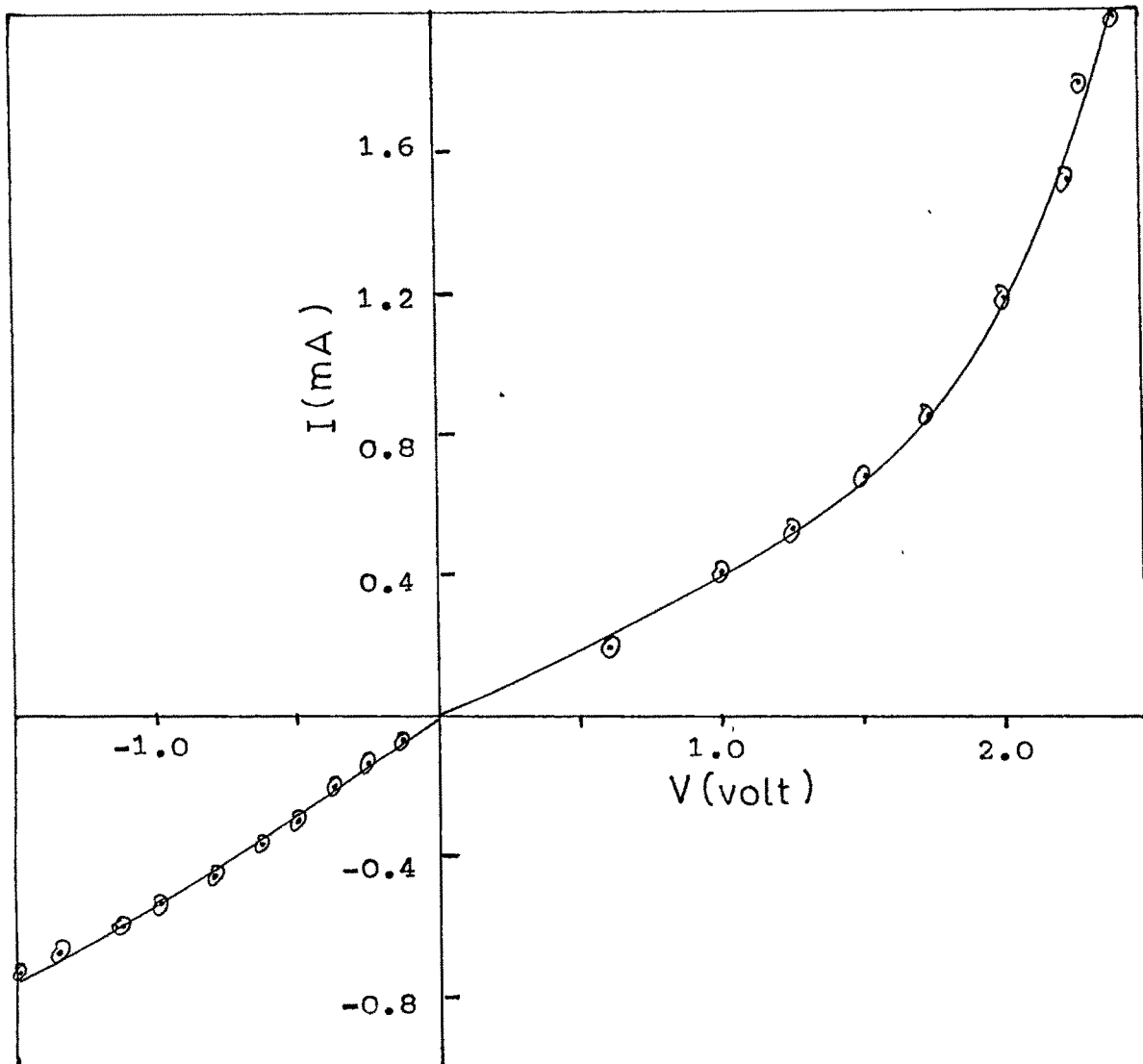


Figure - 19 : I - V characteristic ; Cd/SnSe<sub>2</sub>

TABLE - 2

Junction	$R_s$ (K $\Omega$ )	$R_{sh}$ (K $\Omega$ )	n
In/SnSe	0.1	0.3	4.5
InBi/SnSe	2.0	3.3	11.2
Cd/SnSe <sub>2</sub>	0.7	2.5	10.9

It is worthwhile to note that the ideality factor of In/SnSe is comparable to that of the heterojunctions discussed above. A plot of  $\log I$  vs  $V^{1/2}$  is shown in Figure - 20 for In/SnSe InBi/SnSe and Cd/SnSe<sub>2</sub>. In all the cases a straight line is observed. This indicates Schottky emission to be the dominant electron transfer mechanism in these junctions (2,12,16).

#### C-V Characteristics :

The capacitance of the metal-semiconductor junctions obtained and discussed above was measured at a frequency of 10 KHz on an LCR bridge as a function of applied reverse d.c. bias. The  $1/C^2$  vs  $V$  plots were obtained as straight lines as shown in Figures - 21, 22 and 23, respectively, for In/SnSe, InBi/SnSe and Cd/SnSe<sub>2</sub>. The diffusion potentials of the junctions, obtained as voltage intercepts in these plots are

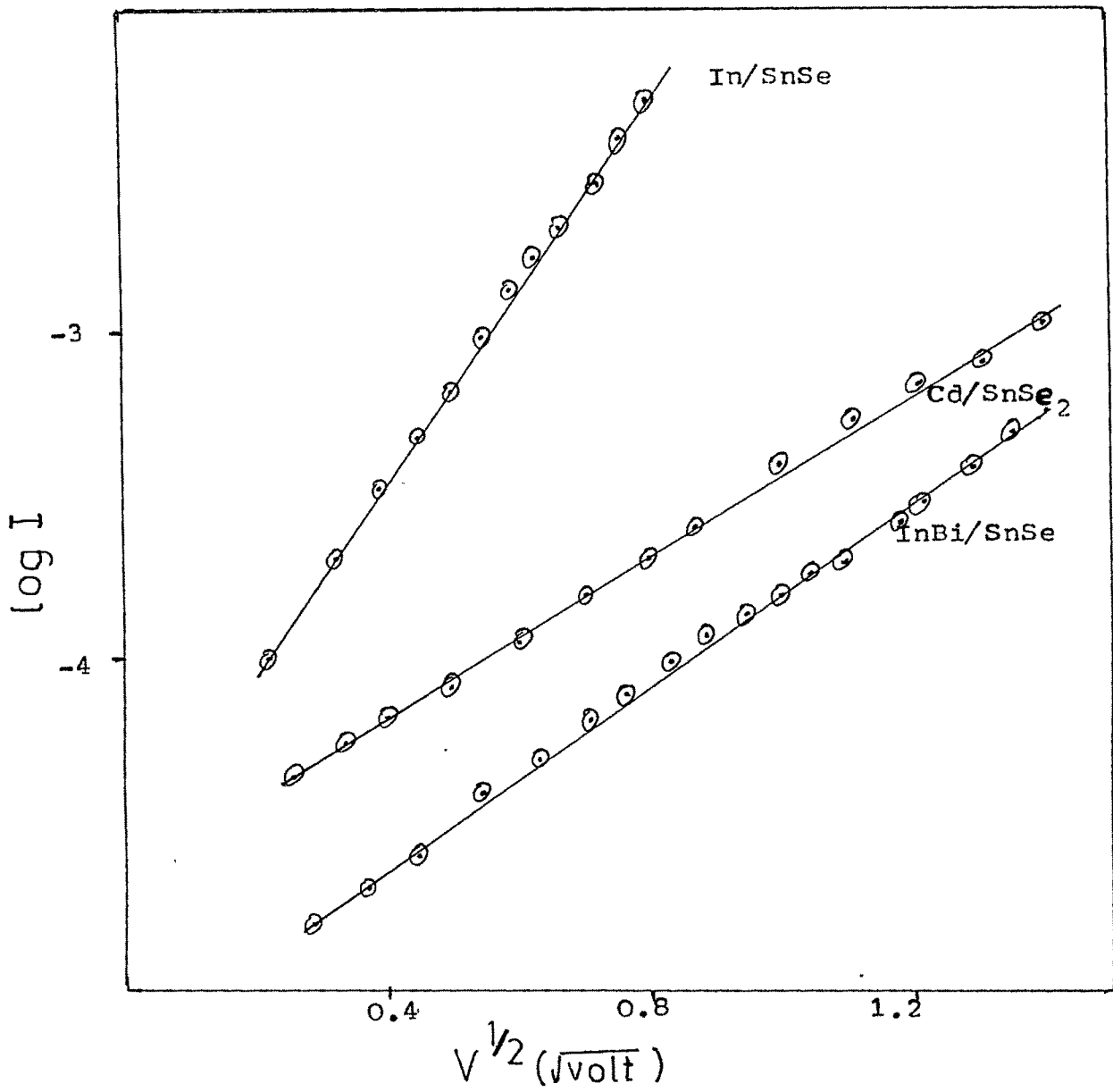


Figure - 20 : Plot of  $\log I$  vs  $V^{1/2}$  of the junctions indicated.

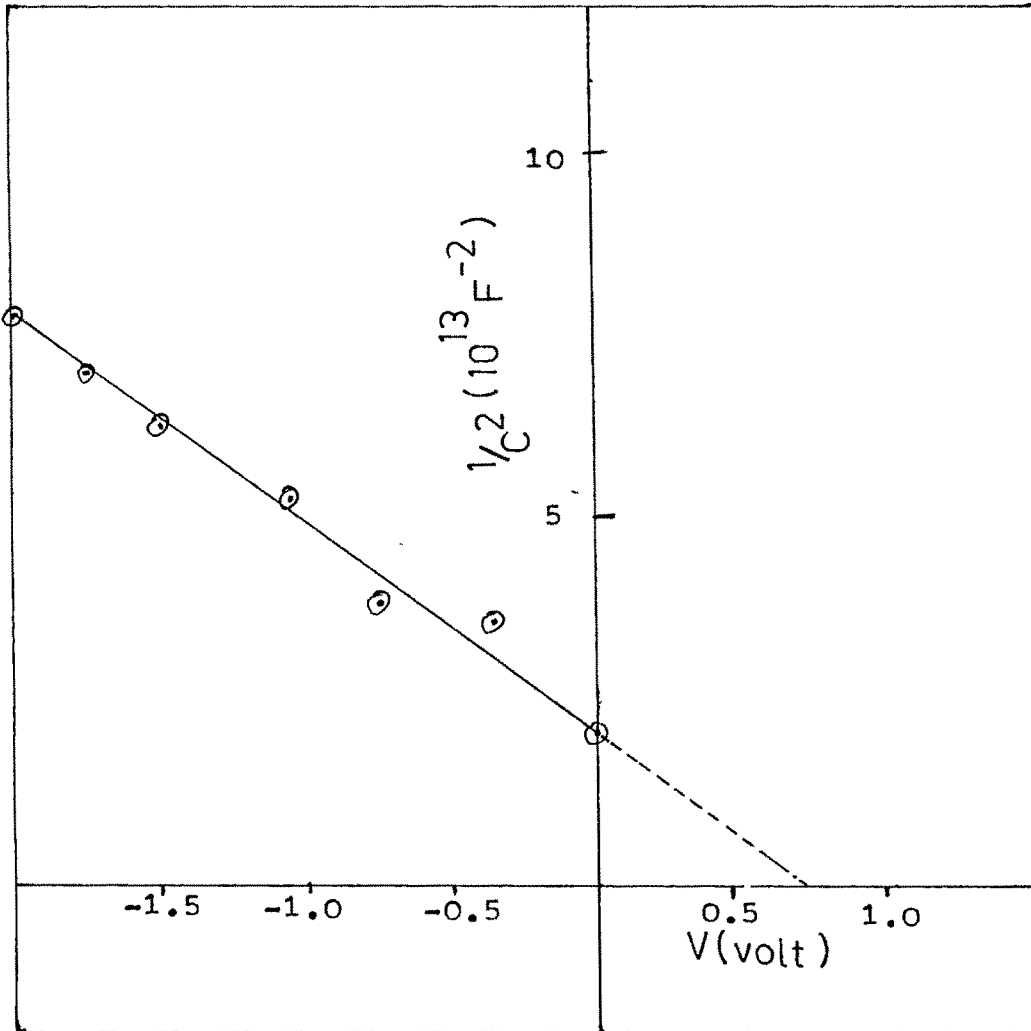


Figure - 21 : Plot of  $1/C^2$  vs  $V$  ; In/SnSe junction.

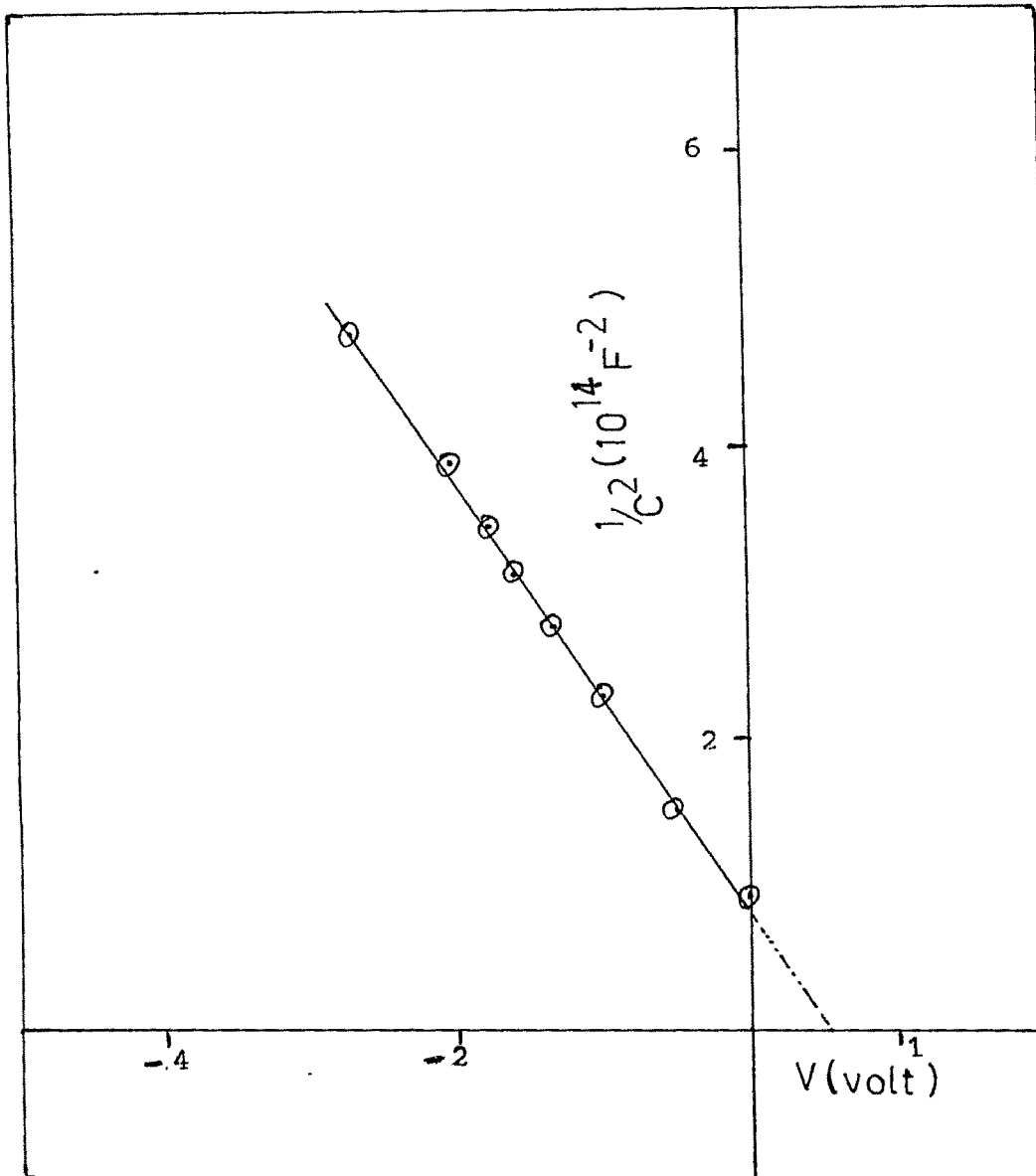


Figure - 22 : Plot of  $1/c^2$  vs  $V$  ; InBi/SnSe junction.

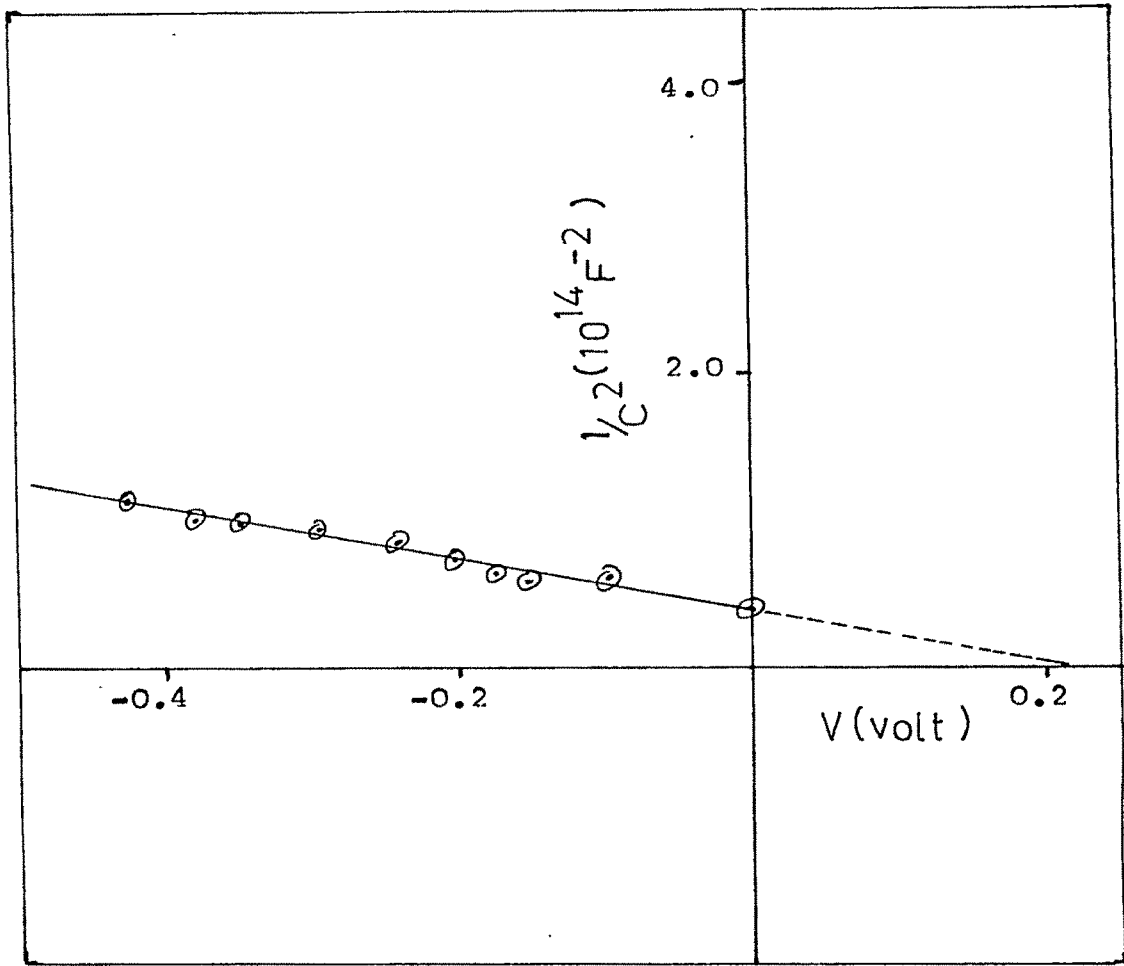


Figure - 23 : Plot of  $1/C^2$  vs  $V$  ; Cd/SnSe<sub>2</sub> junction.

found to be 0.75, 0.5 and 0.23 V, respectively. Again the diffusion potential of In/SnSe, among the three, is the highest and nearly the same as obtained for the heterojunctions discussed above. It is worthwhile to be noticed that the diffusion potential in the case of In/SnSe is significantly higher than reported for the best InP/Au Schottky diodes ; the value in the latter case being 0.52 V<sup>(17)</sup>. However, the ideality factor of In/SnSe is large, if not too large, viz., about 4.5.

#### CONCLUSIONS :

1. Among the three heterojunctions studied, namely, SnSe/SnSe<sub>2</sub>, p-Si/SnSe<sub>2</sub> and n-Si/SnSe, p-Si/SnSe is the best with regard to its  $V_{OC}$ ,  $I_{SC}$ ,  $ff$  and  $n$  which are found to be 189 mV, 0.66  $\mu$ A, 0.67 and 3.8 respectively.
2. The SnSe/SnSe<sub>2</sub> junction has the series resistance less by an order of 100 compared to the report of previous workers. This probably indicates the method of preparing SnSe films by solid state reaction to be superior to the method of compound evaporation.
3. The C - V measurements show that the three junctions studied are all abrupt type and among the three, p-Si/SnSe<sub>2</sub> again has the highest diffusion voltage, namely 0.75 V.
4. The diffusion voltage of the SnSe/SnSe<sub>2</sub> junction

observed in the present case, viz., 0.65 V is also significantly higher than the value reported by previous workers which was about 0.4 V.

5. However, the photovoltaic conversion efficiency of all the three junctions studied are very poor. Yet, among the three, p-Si/SnSe<sub>2</sub> has the highest efficiency.
6. Out of various metal-semiconductor junctions studied, Zn/SnSe, Zn/SnSe<sub>2</sub>, Ni/SnSe<sub>2</sub>, Cd/SnSe and InBi/SnSe<sub>2</sub> are of ohmic nature. Whereas, Cd/SnSe<sub>2</sub>, In/SnSe and InBi/SnSe are found to be of non-ohmic nature.
7. Out of the three non-ohmic metal-semiconductor junctions studied, In/SnSe is observed to be the most promising one due to its highest diffusion voltage, lowest series resistance and lowest ideality factor ; particularly, its diffusion voltage is higher than the value reported for the best InP/Au Schottky diodes.

## REFERENCES :

1. R.H. Bube : Electrons in Solids, Academic press, (London) 1988.
2. S.M. Sze : Physics of Semiconductor Devices, Wiley Eastern limited, New Delhi, (1979).
3. S.J. Fonash : Solar Cell Device Physics, Academic press, New York, (1981).
4. A.L. Fahrenbruch and R.H. Bube : Fundamentals of Solar Cells, Academic Press, New York, (1983).
5. R.H. Bube : Photoconductivity of Solids, John Wiley and Sons Inc., New York (1960).
6. W. Albers and J. Verberkt : J. Mater. Sci. 5 (1970) 24.
7. V.P. Bhatt, Gireesan and C.F. Desai : Indian J. of pure and App. Physics 29 (1991) 27. 500 16 / 119
8. R.Rousina : Ph.D thesis S.P. Univ, Vallabh Vidyanagar, (1988).
9. B.K. Das and S.N. Singh : Photovoltaic Materials and Devices, Wiley Eastern, New Delhi (1985) 281.

10. H.J. Hovel : Semiconductor and Semimetal solar cells, Academic Press, New York, 11 (1975).
11. W. Shockley and R. Henley : Bull. Am. Phys. Soc., 6 (1961) 106.
12. K.L. Chopra, R.Das : Thin Film Solar Cells, Plenum Press, New York, (1983).
13. R.G. Seippel : Photovoltaics, Prentice Hall, Virginia (1983).
14. B. Tuck, G. Eftekhari and D.M. Decogan : J. Phys. D. Appl. Phys. 15 (1982) 457.
15. Ben G. Streatman : Solid State Electronic Devices Prentice Hall of India, New Delhi, 2 (1982) 191.
16. R.Rousina and G.K. Shivkumar : J. Mater. Sci. Letters. 7 (1988) 463.
17. C.Gasnach, S.Cassette, M.A. Di Forepoisson, C.Brylinski, M. Champagne and A. Taodella : Semicond. Sci. Technol. 5 (1990) 322.

S. S. SIDDIQUI, C. F. DESAI, G. R. PANDYA

Physics Department, Faculty of Science  
M.S. University of Baroda, Vadodara, India

Electrical Properties of Thin Films of SnSe-SnSe<sub>2</sub> Eutectic Alloy

Introduction

Among the binary compounds, the group IV chalcogenides have drawn considerable attention of many workers for about the last two decades. The tin chalcogenides have also been studied for their single crystals and thin film growth and also for electrooptic properties (VALIUKONIS et al.; ELKORASHY; GARG et al.; IDEM). There has been an interesting report on the eutectic alloy of SnSe-SnSe<sub>2</sub> (VERBERKT, ALBERS). These authors have studied the lamellar structure of this alloy exhibiting high density multilayered p-n heterojunctions. However, there is no reference found in the literature about any further study on this system. We hereby report the thin film growth of SnSe-SnSe<sub>2</sub> eutectic and the results on electrical conductivity and activation energy of the films of different thicknesses and deposited at different substrate temperatures. Also, the effect of thermal cycling on conductivity has been studied.

Experimental

A mixture of Sn and Se (both 5 N pure) in the ratio of 31 : 69 atomic percentage (VERBERKT, ALBERS) was sealed in a quartz ampoule under a pressure of  $10^{-4}$  Pa. The sealed ampoule was then kept in an alloy mixing furnace, providing rotation and rocking of the charge at 740°C, i.e. 100°C above the melting point (VERBERKT, ALBERS). After 48 hrs of mixing, the molten charge was slowly cooled to room temperature over a period of two days.

Thin films of the alloy obtained were deposited by thermal evaporation on thoroughly cleaned glass substrates in vacuum chamber under a pressure of  $10^{-4}$  Pa. The film thickness was monitored by a quartz crystal oscillator. A radiant heater was used for heat treatment of the substrates and the films inside the vacuum chamber and the temperature was sensed by a chromel-p-alumel thermocouple.

For electrical conductivity measurements of the films, vacuum deposited aluminium was used as ohmic contacts, employing a linear four-probe

arrangement (GOSWAMI, OINA).

Results and discussion

Powdered samples taken from different parts of the alloy ingot were subjected to X-ray diffraction tests. The diffractogram peaks corresponded to SnSe and SnSe<sub>2</sub>. A typical diffractogram is shown by Figure 1.

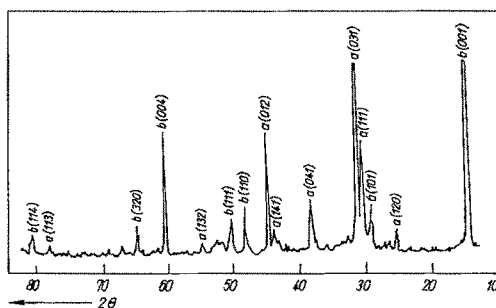


Fig. 1. X-ray diffractogram of SnSe-SnSe<sub>2</sub> eutectic (a - SnSe, b - SnSe<sub>2</sub>)

The peaks were indexed on the basis of the structure and lattice parameters reported by OKAZAKI; MITCHELL, LEVINSTEIN .

Electrical conductivity of the films at different temperatures was measured in the vacuum chamber using digital multimeters. The heating rate of the films was about 5°C/min. The plots of resistivity as a function of temperature for different film thicknesses and substrate temperatures are shown in Figures 2 and 3, respectively.

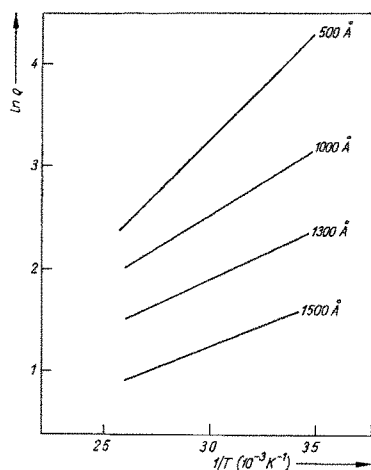


Fig. 2. Plot of  $\ln \rho$  vs  $1/T$  for different thicknesses

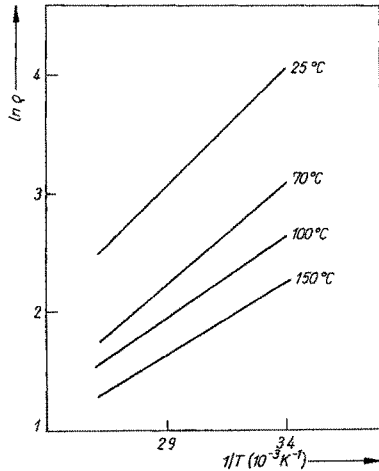


Fig. 3. Plot of  $\ln \rho$  vs  $1/T$  for films obtained at different substrate temperatures

The activation energy for conduction was obtained from these plots and its dependence on film thickness and substrate temperature is shown in Figure 4.

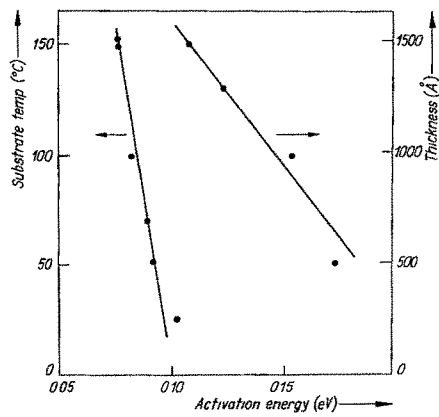


Fig. 4. Plots of activation energy vs film thickness and substrate temperature

The decrease of resistivity and activation energy with increasing substrate temperature indicates the improved crystallinity of the films deposited at increasing temperatures, whereas their decrease with increased film thickness is explained in terms of the films approaching bulk characteristics with increasing thicknesses (SUBBA RAO, CHAUDHARI; DOMINGO et al.; DANGTRAN QUAN).

When subjected to thermal cycling in the range from room temperature to 150°C, the films exhibited fall in resistance by a factor of 100 after

two cycles. However, there was no observable effect of further cycling. A typical plot is shown in Figure 5.

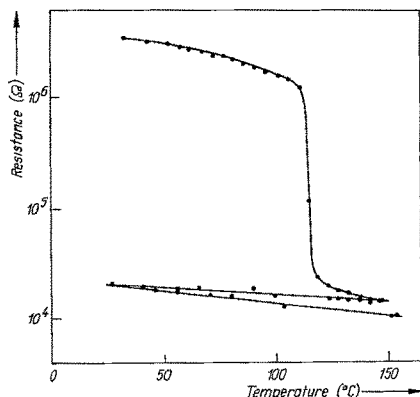


Fig. 5. Thermal cycling curve : resistance vs temperature

It should be noted that such pronounced effect of thermal cycling was observed only in the case of film deposited at room temperature. For the films deposited at temperatures higher than 50°C, there was little or no effect of thermal cycling. This may be because of the amorphous nature of the film deposited at room temperature. This is indicated by abrupt decrease in resistance, observed in the first heating cycle, which may be associated with the onset of recrystallisation of the amorphous film (BHATT, GIREESAN) the onset being at about 110°C in this case, Figure 5.

Authors are grateful to Professor S.K. Shah, the Head of the Physics Department for providing necessary laboratory facilities. They are also grateful to Head, R & D Department, I.P.C.L., Baroda, for obtaining the X-ray diffractograms.

#### References

- BHATT, V.P., GIREESAN, K.: J. Mater. Sci. in electronics 2 (1991) 4  
 DANG TRAN QUAN: phys. stat. sol. (a) 86 (1984) 421  
 DOMINGO, G., ITOGO, R.S., KANNEWURE, C.R.: Phys. Rev. 143 (1966) 536  
 ELKORASHY, A.M.: J. Phys. Chem. Solids 47 (1986) 497  
 GARG, A.K., JAIN A.K., AGNIHOTRI, O.P.: Indian J. Pure Applied Physics 21 (1981) 276  
 GOSWAMI, S.A., OJNA, S.M.: Thin Solid Films 16 (1973) 187  
 IDEM. J. Cryst. Growth 96 (1986) 649  
 MITCHELL, O., LEVINSTEIN, H.: Bull. Amer. Phys. Soc. 6 (1959) 133  
 OKAZAKI, A., UEDA, I.: J. Phys. Soc. Japan 11 (1956) 470  
 SUBBA RAO, T., CHAUDHARI, A.K.: J. Phys. D. Appl. Phys. 18 (1985) 35

VALIUKONIS, G. et al.: phys. stat. sol. (b) 122 (1984) 623

VERBERKT, J., ALBERS, W.: J. Mater. Sci. 5 (1970) 24

(Received June 22, accepted July 9, 1993)

Authors' address:

c/o Dr. C.F. DESAI  
Physics Department  
The M.S. University of Baroda  
Faculty of Science  
Vadodara - 390 002, India

A. D. VLASOV

Cathedra of Physical Chemistry  
 Aviation Institute of Moscow  
 Moscow, Russia

Calculation of the Ideal Tensile Strength of Crystals

1. Introduction

In the previous paper (VLASOV 1990) the non-dislocation model of crystal planes slippage has been proposed. The latter begins when these two planes have diverged to the critical distance by influence of the thermal stress  $\sigma_{th}$ . For this process the simple expression for load/microstrain relation had been derived. The corresponding curve was strikingly alike to the curves obtained in usual tests on metals tensile strength. But the proposed functions for the attraction  $\sigma_E$  and thermal  $\sigma_{th}$  stresses, and for the elasticity modulus  $E$ , being of the real nature, had been given without a substantiation. The same is true for the relation between scale factor  $n$  and microstrain  $\epsilon$ . All of these had resulted in too low critical stresses  $P_n^*$  which correspond with the experimental data for the bulky specimens but do not with the highest tensile strength attainable from some fibres which tend to the ideal tensile strength (MACMILLAN).

2. The basic formulae

Let us to assume Morse potential in the form:

$$U = (E_0/2\varphi^2) \exp(-2\varphi\epsilon) - 2\exp(-\varphi\epsilon) \quad (1)$$

for an interaction between two adjacent infinite crystal planes when these are diverging to a microstrain  $\epsilon = \Delta a/a_0$  where  $a_0$  is the initial distance between these planes and  $\Delta a$  is its increase. In Eq. (1)  $E_0$  is Young's modulus,  $\varphi$  is a constant, Then the attraction stress

$$\sigma_E = dU/d\epsilon = (E_0/\varphi) [1 - \exp(-\varphi\epsilon)] \exp(-\varphi\epsilon) \quad (2)$$

and the elasticity modulus

$$E = d\sigma_E/d\epsilon = E_0 [2\exp(-\varphi\epsilon) - 1] \exp(-\varphi\epsilon) \quad (3)$$

Further, the reason for the thermal stress  $\sigma_{th}$  that appears when crystal planes are diverging, is a heating these planes to the effective temperature  $T_e$  (VLASOV 1986, 1987). Thus

# Optical band gap of thin films of SnSe–SnSe<sub>2</sub> eutectic alloy

S. S. Siddiqui and C. F. Desai

Physics Department, Faculty of Science, Maharaja Sayajinao University of Baroda, Baroda 390002 (India)

(Received May 19, 1993, accepted August 27, 1993)

## Abstract

SnSe and SnSe<sub>2</sub> are known p-type and n-type semiconductors respectively. Following an earlier report on the lamellae-structured SnSe–SnSe<sub>2</sub> eutectic alloy, thin films of this alloy have been prepared. The films exhibit p-type conductivity. From the optical absorbance data, their band gaps have been evaluated and studied as functions of the film thickness and deposition temperature. The data indicate absorbance through indirect intraband transition with a band gap around 1.1 eV. The detailed results are reported

## 1. Introduction

A large number of researchers have shown a considerable interest in the study of binary group IV chalcogenides. Among these, tin chalcogenides in bulk and thin film form have also been studied for their electro-optical properties [1–4]. There has been an interesting report by Albers and Verberkt [5] on the eutectic alloy of SnSe–SnSe<sub>2</sub>, existing in a lamellar form of alternate multilayers. However, no reference has been found in literature about any further study on this system. An X-ray diffraction characterization and electrical conductivity study of its thin films have been reported elsewhere by the present authors [6]. In the present work, our results on the optical properties of SnSe–SnSe<sub>2</sub> eutectic thin films with different thicknesses and those obtained at various substrate temperatures are reported.

## 2. Experimental details

A mixture of Sn and Se (both 99.999% purity) in the ratio of 31:69 (atomic percentage) [5] was sealed in a quartz ampoule under a pressure of 10<sup>-4</sup> Pa. The sealed ampoule was then kept in a mixing furnace at 1013 K, *i.e.* 373 K above the melting point of SnSe–SnSe<sub>2</sub> eutectic [7].

The temperature was controlled by a proportional temperature controller within  $\pm 5$  K. The ampoule was held static for 24 h, and then it was rotated at 1 rev min<sup>-1</sup> and rocked for 24 h. Thereafter it was kept static again for 24 h and was then cooled slowly to room temperature.

Thin films of SnSe–SnSe<sub>2</sub> eutectic were grown on cleaned glass substrates using thermal evaporation in-

side a vacuum chamber under a pressure of about 10<sup>-4</sup> Pa. Films of different thicknesses were deposited at various substrate temperatures using a radiant heater. The temperature was sensed by a chromel–alumel thermocouple. The film thickness was monitored by a quartz crystal film thickness monitor to within 5 nm.

For the optical study, a dual-beam UV–visible–near-IR spectrophotometer (Shimadzu UV-365) was used. The optical gaps were evaluated from the absorbance *vs.* photon energy data for the films deposited at different substrate temperatures and of different thicknesses.

## 3. Results and discussion

The X-ray diffractograms of powders obtained from the bulk alloy and those of the films deposited in different conditions indicated the presence of SnSe and SnSe<sub>2</sub> compound phases in the samples [6].

The optical absorption was measured in the wavelength range from 500 nm to 1500 nm for the films on substrates against a blank substrate as the reference. The absorption coefficient was calculated as a function of photon energy from the absorbance *vs.* wavelength curve.

The plots of  $(\alpha h\nu)^{1/2}$  *vs.*  $h\nu$  were used to evaluate the optical band gaps. A typical plot is shown in Fig. 1 for a film of thickness 100 nm and obtained at 423 K. It can be seen that the plot is linear in the region of strong absorption near the fundamental absorption edge. Thus, the absorption takes place through an indirect intraband transition. The indirect band gap obtained by extrapolating the linear part to the zero of the ordinate is also indicated in the figure. The band gaps  $E_g$  were evaluated in this way for films of different thicknesses  $t$ .

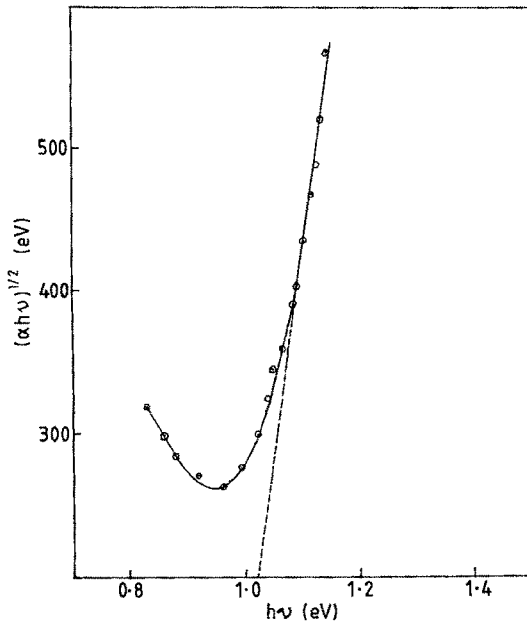


Fig. 1 Plot of  $(\alpha hv)^{1/2}$  vs.  $hv$  for a 100 nm thick film obtained at 423 K

The band gap variation with film thickness follows the relation [8]

$$E_z = \frac{\hbar^2 \pi^2}{2 m^*} \frac{1}{t^2}$$

Here  $m^*$  is the effective mass of the charge carrier,  $t$  is the thickness of the film and  $E_z$  is the kinetic energy contribution due to motion normal to the film plane.

Accordingly, the plot of  $E_g$  vs.  $1/t^2$  is found to be linear (Fig. 2). This variation can be explained in terms of quantum size effect. This is usually defined as the dependence of certain physical properties of a solid on its characteristic geometric dimensions when these dimensions become comparable with the de Broglie wavelength of the charge carriers [9, 10]. Because of the finite thickness of the film, the transverse component of quasi-momentum is quantized. Therefore the electron-hole states assume quasi-discrete energy values in a thin film. As a consequence, the separation of valence and conduction bands increases by an amount  $\Delta E$  given by the above relation. The effective mass of holes calculated from the slope of the  $E_g$  vs.  $1/t^2$  plot (assuming electrons to be heavy) is found to be  $4.4 \times 10^{-4} m_0$ , where  $m_0$  is the electron rest mass. The de Broglie wavelength of the holes, estimated by taking the Fermi energy to be half of the average band gap, turns to be about 85 nm. Thus a quantum size effect is expected to be exhibited by the films.

Films were also deposited at different substrate temperatures ranging from room temperature to 423 K.

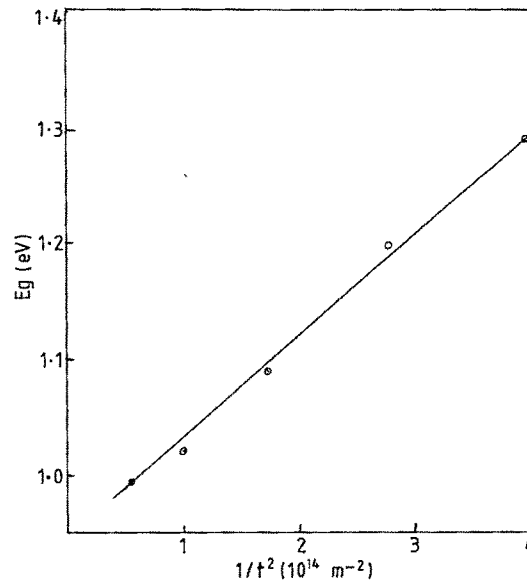


Fig. 2. Plot of band gap vs. inverse square of film thickness obtained at 423 K

However, the band gap did not exhibit any systematic variation except for a general trend of increase. The conductivity type of the films was tested by the hot probe method. Almost all the films exhibited p-type conductivity. It should be noted that SnSe is p type and SnSe<sub>2</sub> n type normally [11–13]. The display of p-type conductivity by film of the eutectic of the two compounds indicates the dominance of tin over selenium [14] in the sample owing to re-evaporation loss of selenium which has a high vapour pressure.

#### 4. Conclusions

The following main conclusions can be drawn from the present study.

- (1) Thin films of SnSe–SnSe<sub>2</sub> eutectic alloy are observed to be p type with an indirect band gap of about 1.1 eV.
- (2) The films with thicknesses of about 100 nm or less exhibit a quantum size effect with respect to optical absorption.
- (3) The deposition temperature does not have a substantial effect on the optical band gap in these films.

#### Acknowledgment

The authors are grateful to Professor S. K. Shah, Head, Physics Department, for providing necessary laboratory facilities.

**References**

- 1 V. P. Bhatt, K. Gireesan and C. F. Desai, *Cryst. Res. Technol.*, **24** (1989) 187
- 2 D. T. Quan, *Phys. Status Solidi A*, **86** (1984) 421
- 3 A. M. Elkovashy, *J. Phys. Chem Solids*, **47** (1986) 497
- 4 A. K. Garg, A. K. Jam and O. P. Agnihotri, *Indian J. Pure Appl. Phys.*, **21** (1983) 276.
- 5 W. Albers and J. Verberkt, *J. Mater. Sci.*, **5** (1970) 24.
- 6 S. S. Siddiqui and C. F. Desai, *Cryst Res Technol*, **28** (1993) K59
- 7 M. Hansen and K. Anderko, *Constitution of Binary Alloys*, McGraw-Hill, London, 1958.
- 8 V. Damodaradas and D. Karunakaran, *J. Appl. Phys.*, **54** (1983) 5252.
- 9 K. L. Chopra, *Thin Film Phenomena*, McGraw-Hill, New York, 1969.
- 10 D. S. Chuu and M. D. Chang, *Phys. Rev. B*, **45** (1992) 11805.
- 11 D. T. Quan, *Thin Solid Films*, **149** (1987) 197.
- 12 G. Domingo, R. S. Itoga and C. R. Kannewurt, *Phys Rev*, **143** (1966) 143.
- 13 T. Subba Rao and A. K. Chaudhari, *J. Phys. D*, **18** (1985) 35.
- 14 D. M. Chizhikov and V. P. Schastilivyi, *Selenium and Selectides*, Collet's, London, 1968